2

POLYMER STATES AND PROPERTIES

J. Betzabe González-Campos, Gabriel Luna-Bárcenas, Diana G. Zárate-Triviño, Arturo Mendoza-Galván, Evgen Prokhorov, Francisco Villaseñor-Ortega, and Isaac C. Sanchez

2.1 INTRODUCTION

Polymers can be either amorphous or semicrystalline in structure. The structure of amorphous materials cannot be described in terms of repeating unit cells such as that of crystalline materials; because of nonperiodicity, the unit cell of an amorphous material would comprise all atoms. The physics and chemistry of the amorphous state remain poorly understood in many aspects. Although numerous experiments and theoretical studies have been performed, many of the amorphous-state features remain unexplained and others are controversial. One such controversial problem is the nature of glass-liquid transition.

Glass transition is a key phenomenon that is useful to understand how external conditions affect physical changes on materials. Theories that predict and describe the glass transition as well as different experimental methods to detect and characterize this phenomenon are of great interest for food, medical, pharmaceutical, and polymer industries [1–4]. It is important to emphasize that the materials of relevance in these industries are interchangeably sharing similar issues on functionality and their association with the glass transition phenomenon.

The glassy state of materials corresponds to a nonequilibrium solid state, in which the molecules forming the material are randomly arranged occupying a volume larger than that of the crystalline state and having a similar composition. Since glassy solids are considered to be in a state of nonequilibrium, the stability of the material is therefore dependent on several factors, which include temperature, water content, molecular weight, and the thermal history undergone by the material before reaching the specific glassy state. The glass transition plays an important role in the stability of various foods and drugs, as well as in polymer manufacturing. Several theories have been developed to understand the glass transition phenomenon from kinetics and thermodynamics standpoints by presenting existing models that are able to estimate the glass transition temperature [1–3]. The development of new materials and understanding the physicochemical behavior of existing ones require a scientific foundation that translates into safe and high quality products with improved quality and functional efficacy of polymers used in different industries.

The glass transition can be measured using different techniques and sometimes they give different results. In the case of chitin (Ch), chitosan (CS), poly(vinyl alcohol) (PVA), and their composites [5–7], improper water elimination analysis had led to a misinterpretation of thermal relaxations, and in some cases, the glass transition phenomenon had not been observed because of this. However, once moisture was properly eliminated, the α-relaxation related to the glass transition phenomenon was revealed [5–7]. In all cases, this behavior was observed through the analysis of their molecular dynamics using dielectric spectroscopy (DS). This is a poorly known tool and not commonly used in the glass transition temperature analysis.

DS has been demonstrated to be a useful tool for the analysis of the glass transition phenomenon in both natural and synthetic polymers, especially under the influence of water, and its application on composites molecular dynamics analysis was also demonstrated [5–7]. This chapter addresses the glass transition phenomenon from an experimental standpoint by exploring a dielectric method used for the characterization of the glass transition phenomenon in natural and synthetic polymers.

Handbook of Polymer Synthesis, Characterization, and Processing, First Edition. Edited by Enrique Saldívar-Guerra and Eduardo Vivaldo-Lima.

2.2 GLASS TRANSITION TEMPERATURE (α-RELAXATION) CONTROVERSY IN CHITIN, CHITOSAN, AND PVA

Solids and liquids are phase separated at the melting point. Polymers have an intermediate boundary called the *glass transition temperature* at which there are remarkable changes in the properties of the polymers. The glass transition temperature (T_g) of a noncrystalline material is the critical temperature at which the material changes its behavior from being "glassy" to being "rubbery." Glassy in this context means hard and brittle (and therefore relatively easy to break), while rubbery means elastic and flexible.

Although fundamentally important, the nature of the glass transition is not well understood. The glass transition is accompanied by significant changes in physical properties such as conductivity and viscosity. Additionally, physicochemical properties of a material such as dissolution, bioavailability, processing, and handling qualities can be related to the material's T_g [8]. Rearrangements that occur in an amorphous material at the glass transition temperature lead to characteristic discontinuities of derivative thermodynamic parameters such as the coefficient of thermal expansion (CTE) or the specific heat. The glass transition temperature can also be considered a measure of compatibility or miscibility in polymer blends.

In polymers, the glass transition phenomenon has been related to the dielectric α-relaxation processes through the Vogel-Fulcher-Tammann (VFT) equation [9], and it can be characterized by means of their molecular dynamics analysis.

In semicrystalline polymers, such as chitin and CS, the value of the glass transition temperature characteristic of the amorphous material was controversial even as to whether polysaccharides exhibit a glass transition temperature (T_g). For many natural polymers, T_g is above the thermal degradation temperature [10]. For chitin, some authors have not observed a glass transition [11], while others report an apparent α-relaxation at 236 °C for α-chitin [12] and 170 °C for β-chitin [13] using DMTA measurements. Lee et al. [14] report an apparent α-relaxation at 182 °C for β-chitin by dielectric measurements.

Regarding CS, some authors using several techniques, including differential scanning calorimetry (DSC) and dynamic mechanical thermal analysis (DMTA), have reported T_g values from 20 to 203 °C [4, 14–18], while others do not observe the glass transition by DSC and DMTA measurements [19]. Some authors have reported molecular dynamics analysis in CS by dielectric measurements with no evidence associated with a glass transition. [19–21] These studies reported local main chain motions at the high frequency side, the β-relaxation process, and at higher temperature the so-called σ-relaxation produced by proton migration [20, 21]. It is well known that this biopolymer is highly hydrophilic and that small amounts of water affect its molecular relaxations. This effect has been reported on wet CS, since it exhibits an additional relaxation referred to as the β_{wet}-relaxation [19–21].

Regarding PVA, it has been shown by DSC, dynamic mechanical analysis (DMA), and DS that the T_g of PVA can be modified by the inclusion of ions, ceramics, monomers, nanoparticles, nanotubes, and other polymers [22–26]. In addition, a plasticizing effect of small amounts of water on T_g could lead to slight differences in the T_g values reported elsewhere [27]. However, most of these analyses were carried out without taking into account the effect of moisture content. In the 30–100 °C temperature range, the temperature dependence of the conductivity and the relaxation time for PVA have been commonly described as Arrhenius-type behavior [28–34]. This behavior can be ascribed to a secondary relaxation process and related to the rotation of hydroxyl groups. Nevertheless, other authors observed a VTF behavior, associated with a primary α-relaxation process [25, 35, 36]. Thermal relaxations of PVA at this temperature range have been subject to contradictory interpretations; therefore, a deep analysis in a wider temperature range is needed to gain a better insight into the molecular dynamics of PVA and its blends, composites, and PVA-based materials.

On the other hand, the physical and chemical properties of polymers can be significantly changed by the presence of small amounts of water [37]; chitin, CS, and PVA have a strong affinity for water and, therefore, can be readily hydrated forming macromolecules with rather disordered structures [38]. A true understanding of hydration properties is essential for several applications in materials science, food industry, and biotechnology [37]. DS is an important technique used to investigate the hydration properties related to the molecular dynamics of materials. The α-relaxation related to the glass transition can be clearly analyzed by this technique. The main advantage of dielectric techniques over others that attempt to measure molecular dynamics is the extremely broad frequency range covered [37]. In this chapter, the glass transition phenomenon is analyzed and described by means of the molecular dynamics analysis.

2.3 GLASS TRANSITION RELATED TO THE α-RELAXATION

The concept of T_g applies only to noncrystalline solids, which are mostly either glasses or rubbers. Noncrystalline materials are also known as *amorphous materials*. Amorphous materials are materials that do not have their atoms or molecules arranged on a lattice that repeats periodically in space. For amorphous solids, whether glasses, organic polymers, or even metals, T_g is the critical temperature that

separates their glassy and rubbery behaviors. If a material is at a temperature below its T_g, large-scale molecular motion is not possible because the material is essentially frozen. If it is at a temperature above its T_g, molecular motion on the scale of its repeat unit (such as a single mer in a polymer) takes place, allowing it to be "soft" or "rubbery." A small change in temperature T_g could result in pronounced changes in the mechanical, thermal, and dielectric properties of amorphous materials.

DSC defines the glass transition as a change in the heat capacity as the polymer matrix goes from the glassy state to the rubbery state. This is a second-order endothermic transition (requires heat to go through the transition), and so in DSC the transition appears as a step transition and not a peak such as might be seen with a melt transition. DSC is the classic and "official" way to determine T_g even though in some cases there are polymeric materials that do not exhibit a sharp T_g by DSC; this has been the case of chitin and CS as well as cellulose [12, 39].

Thermal mechanical analysis (TMA) defines the glass transition in terms of a change in the CTE as the polymer goes from glass to rubber states with the associated change in free molecular volume. Each of these techniques measures a different result of the change from glass to rubber. DSC measures the heat effect, whereas TMA measures the physical effect, that is, the CTE. Both techniques assume that the effect happens over a narrow range of a few degrees in temperature. If the glass transition is very broad, it may not be seen with either approach.

From the practical point of view, fundamental information on the processability of polymers is usually obtained through thermal analysis, which provides knowledge of the main polymer transitions (melting and glass-to-rubber transition to the crystalline and amorphous phases, respectively). In addition to the well-established calorimetric techniques, experimental methods capable of revealing the motional phenomena occurring in the solid state have attracted increasing attention.

In amorphous polymers, α-relaxation, as determined by DS and DMA, corresponds to the glass transition and reflects motions of fairly long chain segments in the amorphous domains of the polymer (long range motions). Relaxations at lower temperatures (labeled β, γ, δ, etc.) are generally due to local movements of the main chain, or rotations and vibrations of terminal groups or other side chains (short range motions). DS and DMA are well-established techniques for the measurement of thermal transitions including the glass transition; they are especially available in detecting T_g of a sample that cannot be observed by normal calorimetric measurements. For example, T_g of polymers having crosslinked network structure [14]. In general, the same relaxation/retardation processes are responsible for the mechanical and dielectric dispersion observed in polar materials [40]. In materials with low polarity, the dielectric relaxations are very weak and cannot be easily detected. However, these two techniques have not been explored at the maximum in relation to the glass transition temperature assignation in natural and synthetic polymers, even though it is demonstrated that they are very effective for the glass transition temperature analysis in hydrophilic polymers [5–7].

The α-relaxation is related to the glass transition of the systems and for that reason this relaxation is also called *dynamic glass transition*. In general, the α-relaxation and the related glass transition phenomenon are not well understood, and the actual microscopic description of the relaxation remains unsolved besides it is a current problem in polymer science [41]. However, it is well accepted that the dynamics of the glass transition is associated with the segmental motion of chains being cooperative in nature [9], which means that a specific segment moves together with its environment. For most amorphous polymers, the α-relaxation has some peculiarities, describe later.

In the α-process, the viscosity and consequently the relaxation time increase drastically as the temperature decreases. Thus, molecular dynamics is characterized by a wide distribution of relaxation times. A strong temperature dependence presenting departure from linearity or non-Arrhenius thermal activation is present, owing to the abrupt increase in relaxation time with the temperature decrease, thus developing a curvature near T_g. This dependence can be well described by the Vogel-Fulcher-Tammann-Hesse (VFTH) equation [40, 41], given by Equation 2.1:

$$\tau = \tau_0 \exp\left(\frac{DT_0}{T - T_0}\right) \tag{2.1}$$

where τ_0 is the pre-exponential factor $\sim 10^{10}$–10^{13} Hz, D is a material's constant, and T_0 is the so-called ideal glass transition or Vogel temperature, which is generally 30–70 K below the glass transition temperature (T_g) [9, 41].

2.4 MOISTURE CONTENT EFFECTS ON POLYMER'S MOLECULAR RELAXATIONS

It is well known that moisture content has a significant influence on chitin, CS, and PVA physical properties [5–7]. A true understanding of hydration properties is essential for several practical applications in materials science, food industry, biotechnology, etc. [42]. CS moisture content is affected by the number of ionic groups in the material as well as their nature. The important binding sites for water molecules in CS are the hydroxyl and amine groups present in the polymer. Several studies have been performed to gain an understanding of the adsorption of water; thermal methods such as thermogravimetry (TGA),

DSC, and dynamical mechanical thermal analysis (DMTA) have emerged as powerful thermoanalytical techniques to monitor physical and chemical changes in both natural and synthetic polymers.

Chitin and CS are a hydrophilic, hence, water-insoluble polysaccharides. The glass transition phenomenon could be also affected by moisture content, since it can work as a plasticizer. Plasticization occurs only in the amorphous region, such that the degree of hydration is quoted as moisture content in the amorphous region. In general, the following three states of water adsorbed on chitin and CS are distinguished:

1. *Nonfreezing Water.* Water that is strongly bound to hydrophilic groups and shows no thermal transition by DSC;
2. *Freezable Bound Water.* Water that is weakly bound to the polymer chain (or weakly bound to the nonfreezing water) and that melts on heating at temperatures greater than 0 °C due to these bonding interactions; and
3. *Free Water.* Water that has the same phase transitions as bulk water.

Polymers that contain the amide group, such as chitin and CS, usually show a low temperature mechanical and dielectric relaxation in the vicinity of −70 °C (at 1 Hz) [43] which is commonly called *water relaxation* since it is sensibly affected by changes in the moisture content of the polymer. Typically the peak intensity, very low when samples are dried, increases with increasing moisture content, whereas correspondingly the peak maximum shifts to lower temperatures. This relaxation has been assigned as the β-wet relaxation attributed to the motion of water–polymer complex in the amorphous regions [20, 21].

Two basic contributions are expected to the variation of dielectric properties of a hydrated material with respect to those of a dry one: that of the polar water molecules themselves and the second one due to the modification of the various polarization and relaxation mechanisms of the matrix material itself by water [37]. In the low frequency region of measurements, there is a third contribution, often ignored in works dealing with high frequency measurements, which arises from the influence of moisture on conductivity and conductivity effects. The increase of electrical conductivity of the sample is the major effect present in wet samples; dielectric response is often masked by conductivity, and it superposes the dielectric processes in the loss spectra and demands a conductivity correction of the dielectric loss spectra [9]. This dc conductivity strongly affects the modified loss factor, ε''. In this case, it can be expressed as shown in the following equation:

$$\varepsilon'' = \varepsilon''_{\text{exp}} - \frac{\sigma_{\text{dc}}}{\omega \varepsilon_0} \tag{2.2}$$

In Equation 2.2, $\varepsilon''_{\text{exp}}$ is the experimental loss factor value; σ_{dc} is direct current conductivity; d and S are thickness and area of sample, respectively; $\omega = 2\pi f$ (f is frequency); and ε_0 is the permittivity of vacuum. As a general rule for polymers, σ_{dc} is determined from fitting of the real component of the complex conductivity ($\sigma_{\text{dc}} = \sigma_0 f^n$, where σ_0 and n are fitting parameters) measured in the low frequency range where a plateau is expected to appear.

However, generally in composites with conductive inclusions, ionic current and interfacial polarization could often mask the real dielectric relaxation processes in the low frequency range. Therefore, to analyze the dielectric process in detail, the complex permittivity ε^* can be converted to the complex electric modulus M^* by using the following equation:

$$M^* = \frac{1}{\varepsilon^*} = M' + iM'' = \frac{\varepsilon'}{\varepsilon'^2 + \varepsilon''^2} + \frac{\varepsilon''}{\varepsilon'^2 + \varepsilon''^2} \tag{2.3}$$

where M' is the real and M'' the imaginary parts of electric modulus, and ε' is the real and ε'' the imaginary parts of permittivity.

Interpreting the experimental data in this form nowadays is a commonly employed method to obtain information about the relaxation processes in ionic conductive materials and polymer-conductivity nanoparticles composites. In this representation, interfacial polarization and electrode contributions are essentially suppressed [44, 45]. The peak in the imaginary part of M'' depends on temperature, which can be related to the translational ionic motions. The corresponding relaxation time $\tau_\sigma = 1/(2\pi f_{\text{p}})$, where f_{p} is the peak frequency, therefore is called *conductivity relaxation time*.

In this case, this chapter presents both analyses; in the case of chitin and CS, the analysis by means of the real (ε') and the imaginary (ε'') parts of permittivity and for PVA the case of the analysis by the complex electric modulus, M^*.

2.5 DIELECTRIC FUNDAMENTALS

DS measures the dielectric permittivity as a function of frequency and temperature. It can be applied to all nonconducting materials. The frequency range extends over nearly 18 orders in magnitude: from the microhertz to terahertz range close to the infrared region. This remarkable breadth is the key feature that enables one to relate the observed dielectric response to slow (low frequency) and/or fast (high frequency) molecular events. DS is sensitive to dipolar species as well as localized charges in a material; it determines their strength, kinetics, and interactions. Thus, DS is a powerful tool for the electrical characterization of nonconducting materials in relation to their structure.

2.5.1 The Origin of Dielectric Response

When a metal body is exposed to an electric field, free electrons are displaced by electric forces until the field in the body vanishes. In an ideal dielectric (dc conductivity is zero), there exists only bound charges (electrons, ions) that can be displaced from their equilibrium positions until the field force and the oppositely acting elastic force are equal. This phenomenon is called *displacement polarization* (electronic or ionic polarization). A dipole moment is induced in every atom or between ion pairs. The molecular dipoles can only be rotated by an electric field. Usually, their dipole moments are randomly oriented. In an external field, however, an orientation parallel to the field direction is preferred so that a dipole moment is induced. This process is called *orientational polarization*.

In an alternating electric field, the displacement polarization leads to electric oscillations. This is a resonant process with resonant frequencies of $10^{15}-10^{14}$ Hz for the electronic and of $10^{13}-10^{12}$ Hz for the ionic polarization.

Orientational polarization is not a resonant process since the molecular dipoles have inertia. The response of the orientational polarization to a charge of the electric field is, therefore, always retarded. This process is called *dielectric relaxation*. The characteristic time constant of such a relaxation process—this is the time for reaching new equilibrium after changing the excitation—is called *relaxation time* (τ). It is strongly temperature dependent, since it is closely related to the viscosity of the material. At room temperature, the relaxation times of the orientational polarization in crystals are of $10^{-11}-10^{-9}$ s. In amorphous solids and polymers, however, they can reach a few seconds or even hours, days, and years, depending on the temperature.

In polymer materials that are studied by DS, there are two major polarization mechanisms: (i) polarization due to charge migration and (ii) polarization due to the orientation of permanent dipoles. Let us look at charge migration first. Migration of charges gives rise to conductivity [20]. The measured conductivity encompasses contributions from extrinsic migrating charges (e.g., ionic impurities) and intrinsic migrating charges (e.g., proton transfers along hydrogen bonds). Regarding dipole orientation, while electronic and atomic polarization result from induce dipoles, there are many materials that contain permanent dipoles. When such materials are placed in the electric field, dipole orientation or dipole polarization is produced as a result of the alignment of dipoles in the direction of the applied field. The orientation (polarization) of permanent dipoles involves cooperative motions of molecular segments in a viscous medium with time-scales measurable by DS.

Real dielectrics also contain charge carriers that can be moved by electric forces between potential walls, formed by non-ohmic or blocking contacts or internal boundaries, for example, between crystalline and amorphous phases in a semicrystalline material. This leads to a space charge polarization (electrode polarization or Maxwell–Wagner polarization, respectively), which on the other hand is limited by diffusion. These processes are also relaxation processes and are called *charge-carrier relaxations*. Because these processes are closely related to the conductivity, they are sometimes also named *conductivity relaxations*.

The dielectric (ε^*) and loss (ε'') constants are important properties of interest because these two parameters, among others, determine the suitability of a material for a given application. Dielectric relaxations are studied to reduce energy losses in materials used in practically important areas of insulation and mechanical strength.

2.5.2 Dielectric Relaxation in Solid Polymers

Several and different relaxation processes are usually present in solid polymeric materials, and these are dielectrically active if they incur significant orientation of molecular dipoles. The multiplicity of relaxation process is seen most easily in a scan dielectric loss at constant frequency as a function of temperature. As temperature is raised, molecular mobilities of various types become successively energized and available for dipolar orientation. By convention, the dielectric relaxation processes are labeled α, β, and so on, beginning at the high temperature end. The same relaxation processes are generally responsible for dispersions in mechanical properties too, although a particular molecular rearrangement process may produce a stronger dielectric than mechanical effect or vice versa [40].

Some polymers are completely amorphous, and there is only one phase present in the solid material. In such cases, there is always a high temperature α-relaxation associated with the micro-Brownian motion of the whole chains and, in addition, at least one low temperature (β, γ, etc.) subsidiary relaxation. The relative strength of the α- and β-dielectric relaxations depends on how much orientation of the dipolar groups can occur through the limited mobility allowed by the β-process before the more difficult but more expensive mobility of the α-process comes into play: there is a partitioning of the total dipolar alignment among the molecular rearrangement processes.

A detailed examination of the relaxations requires isothermal scans of relative permittivity and dielectric loss factor as a function of frequency, f, so that the effective dipole movements and activation energies of relaxation times may be obtained. A typical pair of plots of ε'' and ε' values against log f is shown in Figure 2.1. Plots of dielectric data of this kind are sometimes called *dielectric spectra*. From a series of such plots, the relaxation times can be obtained for the individual relaxation processes as a function of temperature.

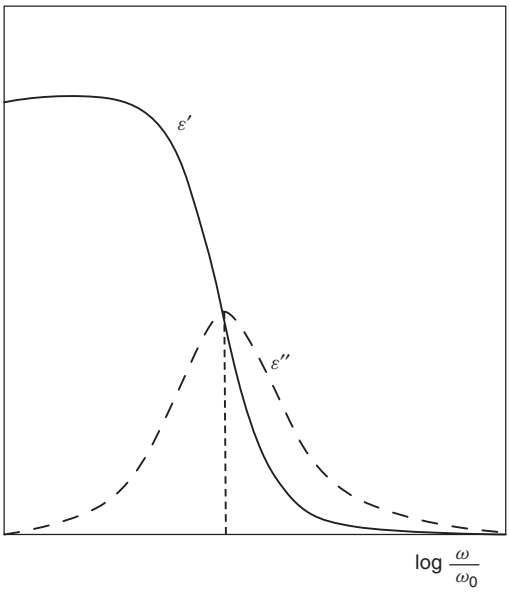

Figure 2.1 Dielectric relaxation curves commonly found in dielectric processes.

Molecular processes cover a broad frequency range being associated with the length scale of the conformational mobility in the polymeric chain. Hence, relaxation processes in polymeric materials involve hierarchy that goes from very local motions (β, δ, γ, etc.) to segmental mobility involving cooperativity (α-process), or even relaxation processes involving large or complete polymeric segments [40].

When studying a polymer on a large frequency/time scale, the response of a given material under a dynamic stimulus usually exhibits several relaxations. Moreover, the peaks are usually broad and sometimes and are associated with superposed processes. The relaxation rate, shape of the loss peak, and relaxation strength depend on the motion associated with a given relaxation process [41]. In general, the same relaxation/retardation processes are responsible for the mechanical and dielectric dispersion observed in polar materials [40]. In materials with low polarity, the dielectric relaxations are very weak and cannot be easily detected. The main relaxation processes detected in polymeric systems are analyzed next.

2.5.3 α-Relaxation

The α-relaxation and its features were described in Section 2.4. As mentioned before, a strong temperature dependence presenting departure from linearity or non-Arrhenius thermal activation is present as shown in Figure 2.2, due to the abrupt increase in relaxation time with the temperature decrease, thus developing a curvature near T_g. This dependence can be well described by the VFTH equation.

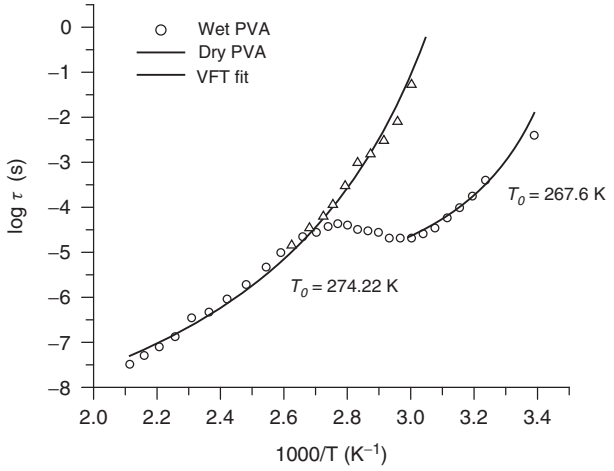

Figure 2.2 Relaxation time (τ) versus 1000/T for PVA disclosing the α-relaxation obtained by dielectric spectroscopy. The solid line is the VFTH fitting of the dielectric data. *Source*: Reproduced with permission from González-Campos JB, García-Carvajal ZY, Prokhorov E, Luna-Bárcenas JG, Mendoza-Duarte ME, Lara-Romero J, Del Río RE, Sanchez IC. J Appl Polym Sci 2012;125:4082 [7]. Copyright 2012 John Wiley and Sons, Inc.

In general, the α-process is well defined in the frequency domain and shows a relatively broad and asymmetric peak. Several functions such as the Cole–Cole and Cole–Davison in the frequency domain are able to describe broad symmetric and asymmetric peaks. The most general one is the model function of Havriliak and Negami (HN function) [41].

2.5.4 β-Relaxation

Localized motions, involving either in-chain movements or side groups laterally attached to the main chain, are the origin this process. This type of local dynamic stays active even when the polymer is in the glassy state [40], that is, when the large length scale backbone motions are frozen.

This process is thermally activated and the temperature dependence of the relaxation rate is found to be Arrhenius-like, that is,

$$\tau = \tau_0 \exp^{\Delta E_a/RT} \tag{2.4}$$

where τ_0 is the pre-exponential factor and E_a is activation energy. For truly activated process, τ_{dc} should be of the magnitude of 10^{12}–10^{13} Hz. The activation energy is associated with the slope of log τ_{dc} versus $1/T$ and depends on both, the internal rotation barriers and the environment of a moving unit.

In the frequency domain, the dielectric β-relaxation displays a broad and in the most cases symmetric loss peak with half widths of four to six decades [41]. The variety of molecular environments (structural heterogeneity) of the

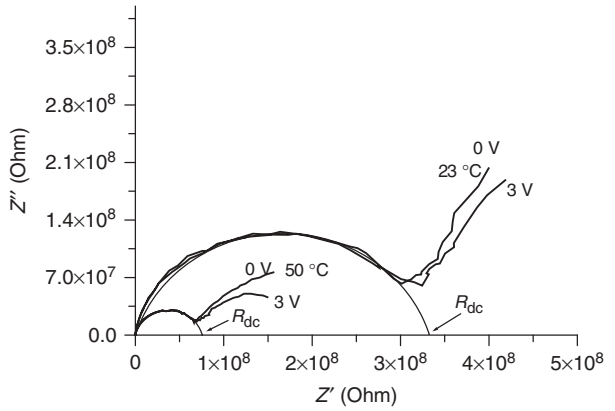

Figure 2.3 Dielectric spectra of wet chitin films at different bias applied voltage. Contact effect is observed when applied voltage is changed from 0 V to 3 V in the quasilinear response (outside the semicircle). *Source*: Reproduced with permission from González-Campos JB, Prokhorov E, Luna-Bárcenas G, Mendoza-Galván A, Sanchez IC, Nuño-Donlucas SM, García-Gaitan B, Kovalenko Y. J Polym Sci B Polym Phys 2009;47:932 [5]. Copyright 2009 John Wiley and Sons, Inc.

relaxation unit and, consequently, a variety of energy barriers contribute to the extremely broad peak developing [40]. Generally, dielectric strength ($\Delta\varepsilon_\beta$) increases with temperature and it is much lower in the β-relaxation process, relatively to the α-process. The relative strength depends on how much orientation of the dipolar groups can occur through the limited mobility allowed by the β-process.

2.5.5 dc Conductivity Calculation

The dc conductivity (σ_{dc}) of polymer's films can be calculated by dielectric measurements using the methodology previously described by González-Campos et al. [5, 6]. R_{dc} is obtained from the intersection of the semicircle and the real-part axis on the impedance plane ($Z'' = 0$); σ_{dc} can be calculated by the following relationship: $\sigma_{dc} = d/(R_{dc} \times A)$, where d is the thickness and A the area of the film.

In chitin, CS and PVA complex dielectric spectra (Z'' versus Z' plot shown in Fig. 2.3), two different behaviors are identified: (i) a typical semicircle at "high" frequencies, which corresponds to the bulk material signal and (ii) a quasilinear response at "low" frequencies associated with interfacial polarization in the bulk of the films and/or surface and contact effects [46, 47]. This low frequency part of the electrical response is easily influenced by imperfect contact between the metal electrode and the sample; as it was previously tested elsewhere [5], there is no influence of gold contact on the polymer impedance spectra (high frequency part of the spectra corresponding to the bulk of the film) and it is discarded for further analysis.

2.6 CHITIN, CHITOSAN, AND PVA FILMS PREPARATION FOR DIELECTRIC MEASUREMENTS

2.6.1 Chitin Films Preparation

Chitin was purchased from Sigma-Aldrich (1.2% of ash content, 96% degree of acetylation, and bulk density of 1.425 g/ml). Chitin was purified according to the procedure reported in Reference 48. The viscosity average molecular weight, $\overline{M_v} = 300{,}000$, was determined according to Mirzadeh et al. [49] by means of the Mark–Houwink relationship. Hexafluoroisopropanol (HFIP) was purchased from Sigma-Aldrich and was used as received. Chitin was dissolved in HFIP to prepare a 0.5% w/v solution. This solution was magnetically stirred for 24 h to promote chitin dissolution. Films were prepared by the solvent cast method by pouring the solution into a plastic Petri dish and allowing the solvent to evaporate at room temperature.

2.6.2 Neutralized and Nonneutralized Chitosan Films Preparation

CS medium molecular weight (Mw = 150,000 g/gmol) and 82% of degree of deacetylation (DD) reported by the supplier and calculated according to Reference 49 was purchased from Sigma-Aldrich. Acetic acid from J. T. Baker was used as received without further purification. CS films were obtained by dissolving 1 wt% of CS in a 1 wt% aqueous acetic acid solution with subsequent stirring to promote dissolution. As chitin films, CS films were prepared by the solvent cast method by pouring the solution into a plastic Petri dish and allowing the solvent to evaporate at 60 °C. CS films prepared from acetic acid solution have the amino side group protonated (NH_3^+ groups); therefore, the films need to be neutralized. The films were immerse into a 0.1 M NaOH solution for 30 min and washed with distilled water until neutral pH; a subsequent drying step in furnace at 130 °C for 14 h was needed. The results of both neutralized as well as nonneutralized CS films are shown.

PVA, Mw ≈ 89,800–98,000 g/mol and hydrolysis degree >99%, was purchased from Sigma-Aldrich and used as received. PVA films were obtained by dissolving a known amount of PVA in water to obtain a 7.8 wt% solution under stirring. Films were prepared by the solvent casting method, by pouring the former solution into plastic Petri dishes and allowing the solvent to evaporate at 60 °C.

These films had thicknesses of circa 40 μm measured by a Mitutoyo micrometer. A thin layer of gold was vacuum deposited onto both film sides to serve as electrodes. Rectangular small pieces (4 mm × 3 mm) of these films were prepared for measurements and the contact areas were measured with a digital calibrator (Mitutoyo).

2.6.3 Electrode Preparation for Dielectric Measurements

In both chitin and CS films, a thin layer of gold was vacuum deposited onto both film sides to serve as electrodes, using a device (Plasma Sciences Inc.) with a gold target (Purity 99.99%) and Argon as gas carrier. Gas pressure was set to 30 mTorr and voltage to 0.2 kV. Sputtering time was 4 min onto each side. Rectangular small pieces (5 mm × 4 mm) of these films were prepared for dielectric measurements. The contact area and thickness were measured with a digital calibrator (Mitutoyo) and a micrometer (Mitutoyo), respectively. This method allows obtaining films of circa 10 μm of thickness.

2.7 DIELECTRIC RELAXATIONS IN CHITIN: EVIDENCE FOR A GLASS TRANSITION

2.7.1 Effect of Moisture on Dielectric Spectra

Figure 2.4 shows the dependence of dc resistance, capacitance, and weight loss (TGA measurements) versus temperature for wet chitin (12.3% water). It can be observed that in the temperature range 20–80 °C the resistance increases, and capacitance and weight rapidly decrease. This behavior is caused by a water modification effect on the relaxation mechanism of the matrix since water has a lower resistance and higher dielectric constant. When water is present, biopolymer's resistance decreases; if temperature increases, water evaporates and resistance increases (weight loss in the TGA measurements is registered). When water content is nearly zero (dry annealed), the real dielectric behavior of chitin is revealed. Films with near zero moisture content exhibit higher resistances at room temperature and lower resistance as temperature increases (see window inset in Fig. 2.4, dry annealed film). In summary, to obtain the dielectric behavior of pure chitin without moisture influence, it is necessary to evaporate it by annealing; otherwise, its evaporation may mask the electrical properties of the biopolymer.

For dry chitin films, we emulated dielectric measuring conditions for TGA measurements: after overnight annealing in an oven at 120 °C, these films were handled in ambient conditions for 10–15 min for TGA measurements (time to weight samples for TGA ∼ time for sample handling prior to dielectric measurements). The weight loss, and therefore moisture content, is circa 3.5% (Fig. 2.5), which indicates that chitin reabsorbs water readily during the 10–15 min handling from the oven to the vacuum cell. Hence, a second heat treatment in the vacuum cell before dielectric measurements is needed. These films were reheated at 120 °C in the impedance vacuum cell for 1 h (dry annealed films).

As illustrated in Figure 2.5, the water content in chitin films is circa 12.3% as calculated by TGA. These films were kept at normal ambient conditions before dielectric and TGA measurements and were designated as wet samples. This moisture content is in agreement with those reported for chitin and CS [17, 19, 49].

After this annealing step, no resistance change is observed, indicating that the residual water has been removed. This fact is clearly shown by the Cole–Cole plot in Figure 2.6a. Here, the change of Z'' versus Z' with thermal treatment is greatly affected by its water content. It is noteworthy that the wet chitin sample with no heat treatment shows a completely different behavior as compared to the thermally treated samples. On the other hand, Figure 2.6b shows the commonly used ε'' versus frequency plot after dc conductivity correction in the low frequency part of the spectra, and as can be seen, no clear change with heat treatment can be detected; this is

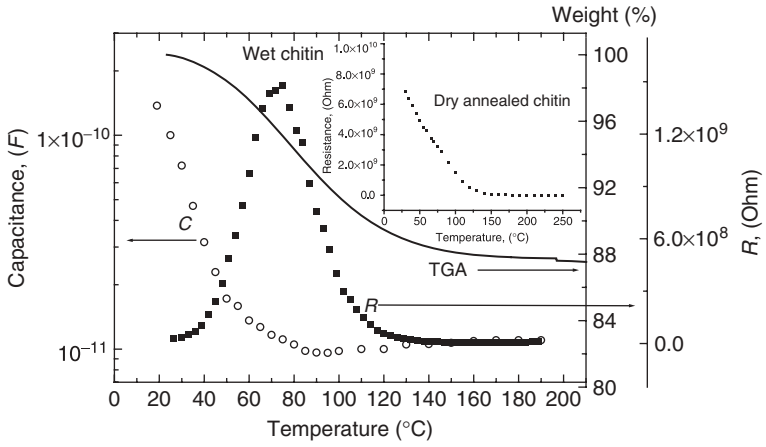

Figure 2.4 Resistance (solid squares) and capacitance (open circles) as a function of temperature for wet film. Thermogravimetric response is also shown. Note that as temperature increases resistance increases due to water evaporation and finally decreases. Window inset shows the opposite behavior for dry film after water evaporation by annealing.

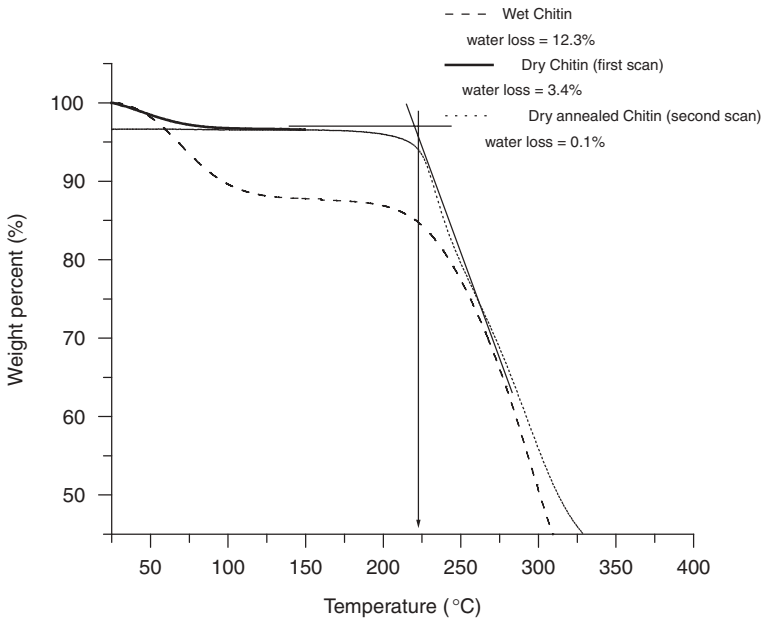

Figure 2.5 Thermogravimetric analysis of solvent-cast α-chitin films. Wet chitin (solid line), dry chitin: first scan (dashed line), and dry annealed chitin: second scan (dash-dotted line) from 20 to 250 °C. Note that above 210 °C α-chitin thermally decomposes. A construction of tangent lines is operationally used to determine the onset of degradation (circa >210 °C). *Source*: Reproduced with permission from González-Campos JB, Prokhorov E, Luna-Bárcenas G, Mendoza-Galván A, Sanchez IC, Nuño-Donlucas SM, García-Gaitan B, Kovalenko Y. J Polym Sci B Polym Phys 2009;47:932 [5]. Copyright 2009 John Wiley and Sons, Inc.

a critical issue since moisture effects are observable in one representation of the dielectric data, but not in the other.

These films are cooled under vacuum from 120 °C to room temperature (20 °C) and then a second measurement is performed in the dry annealed films. To calculate water content on these films, TGA measurements were performed in dry samples (heated at 120 °C in oven overnight). After 1 h at 120 °C (dry annealed films), no further change in weight is observed; the films were cooled to 20 °C and reheated. The second TGA scan for dry annealed chitin films shows free water content of circa 0.1% (dash-dotted line, Fig. 2.5). Using the same annealing methodology in the dielectric and TGA measurements, we can monitor the water content in the samples.

Modulated DSC thermograms (Fig. 2.7) for chitin films after water removal were scanned a second time from 20 to 250 °C. The objective was to see whether a glass transition would manifest. However, as stated in Section 2.1, controversy centers on whether a glass transition can be detected. In our case, there is no clear evidence of the glass transition; hence, it is not possible to draw any conclusion from the thermal analysis. As explained earlier, some authors assign no T_g for chitin [11], while others [12] assign approximately 236 °C for β-chitin, which is in chitin's degradation temperature range (210–280 °C). As can be seen in Figure 2.5 by TGA measurements, the onset of degradation is about circa 220 °C from the intersection of two tangent lines (by DSC the onset of degradation is circa 210 °C). Other authors report a surprisingly high value of T_g of 350–412 °C for β-chitin, which has a degradation temperature of 450 °C [50].

2.7.2 X-Ray Diffraction Measurements

Crystal structure analysis was performed using a 2100-Rigaku diffractometer equipped with the CuK α radiation ($\lambda = 1.5406$ Å) in the 2θ range from 5° to 55°, at 30 and 120 °C and operating at 30 kV and 16 mA.

It is well known that chitin is a semicrystalline polymer. Consequently, it is necessary to verify whether chitin's crystalline volume fraction changes with heat treatment and its influence on relaxation behaviors. The diffraction pattern of purified α-chitin powder is shown in Figure 2.8. The five characteristic crystalline reflections for α-chitin are present [51]. They are indexed as (020), (110), (120), (101), and (130) for 9.24°, 19.13°, 20.5°, 23.31°, and 26.2°, respectively. α-Chitin has an orthorhombic unit cell with P212121 symmetry [52], indicating an antiparallel arrangement of the chitin chain with intermolecular hydrogen bonding. The peak at $2\theta = 9.24°$ is associated with the most ordered regions involving the acetamide groups [53]. The strongest reflection of an α-chitin crystalline sample is obtained at $2\theta = 19.13°$.

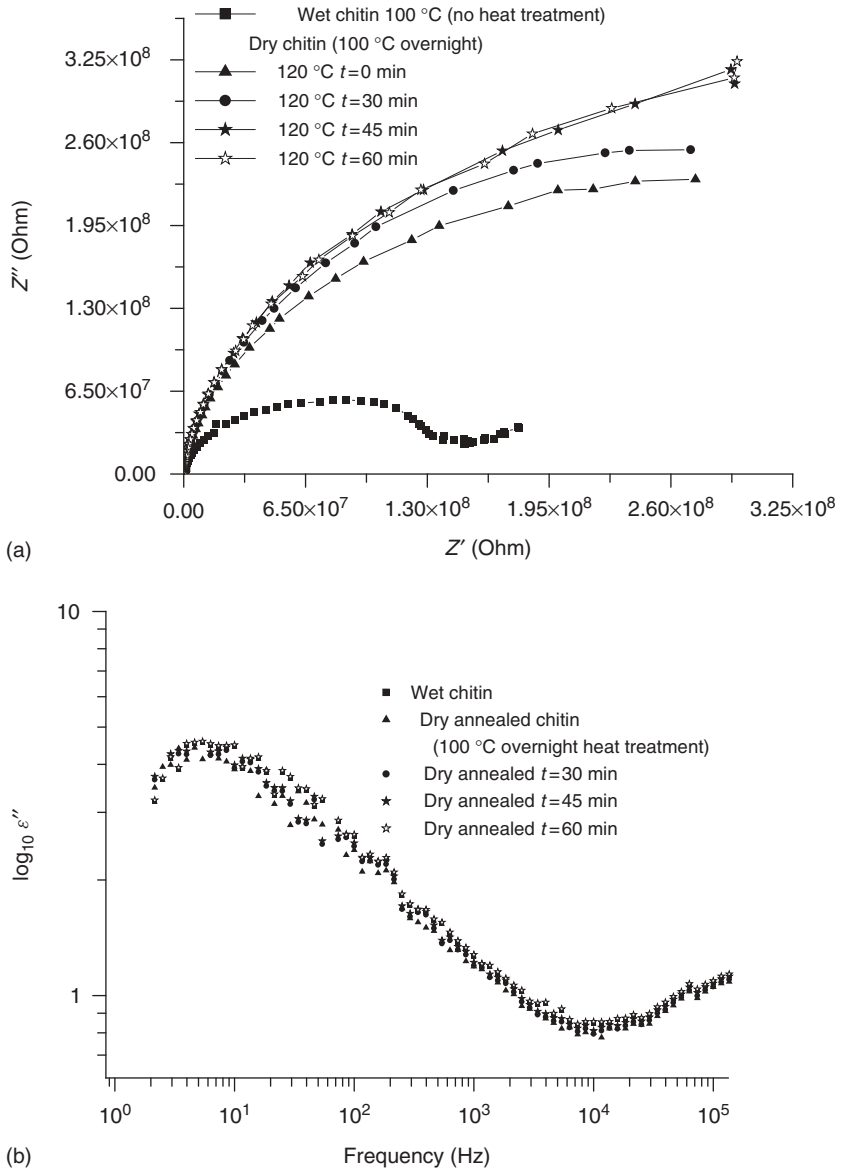

Figure 2.6 (a) Cole–Cole plot for chitin under second heat treatment in vacuum cell. Water completely drives off after 1 h evidenced by no resistance change. (b) log 10 ε'' versus frequency for chitin in vacuum cell; the data were corrected for dc conductivity contribution. Note that conventional plots of log ε'' versus frequency do not show a clearly change in function of time after water removal. *Source*: Reproduced with permission from González-Campos JB, Prokhorov E, Luna-Bárcenas G, Mendoza-Galván A, Sanchez IC, Nuño-Donlucas SM, García-Gaitan B, Kovalenko Y. J Polym Sci B Polym Phys 2009;47:932 [5]. Copyright 2009 John Wiley and Sons, Inc.

The estimation of crystalline volume fraction was based on the standard approach that assumes the fact that the experimental intensity curve is a linear combination of intensities of crystalline and amorphous phases. For bulk α-chitin, the crystalline volume fraction is about 30% and about 10% for film samples. A similar behavior was found for CS acetate after dissolution into acid solutions [54]. The films crystalline volume fraction does not change after annealing at 120 °C, and so the amorphous phase volume fraction is constant during the dielectric measurements at the annealing temperature employed. In subsequent analyses, we make the usual assumption that crystalline units are immobile relative to amorphous units and do not contribute to relaxations.

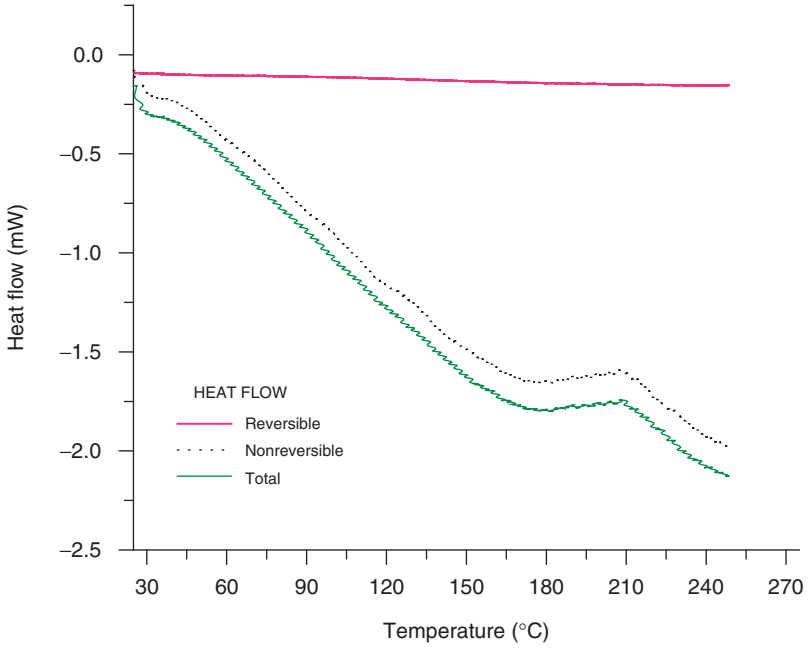

Figure 2.7 DSC analysis for chitin films.

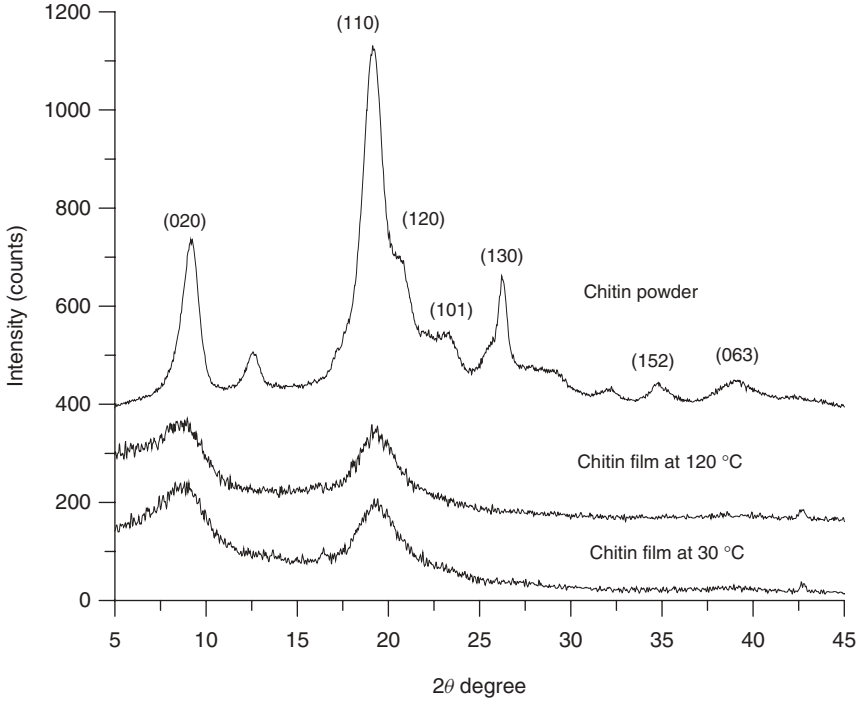

Figure 2.8 X-Ray diffraction pattern for (powder and film) α-chitin. *Source*: Reproduced with permission from González-Campos JB, Prokhorov E, Luna-Bárcenas G, Mendoza-Galván A, Sanchez IC, Nuño-Donlucas SM, García-Gaitan B, Kovalenko Y. J Polym Sci B Polym Phys 2009;47:932 [5]. Copyright 2009 John Wiley and Sons, Inc.

2.7.3 Dielectric Spectra: General Features

Figure 2.9 shows the complex Cole–Cole plot for wet (Fig. 2.9a) and dry annealed chitin films (Fig. 2.9b) measured at 25, 50, 70, and 130 °C, respectively. A Cole–Cole type plot of Z'' versus Z' for wet films exhibit characteristic semicircles at high frequencies and a quasilinear response at low frequencies. This behavior is due to the presence of water in the samples, that is, water reduces the resistivity of films and could be modifying the relaxation mechanism of the matrix material.

However, for dry annealed samples (Fig. 2.9b), the semicircle is not fully resolved due to an increase in film's resistivity at 25 °C. As temperature increases, resistivity decreases and the full semicircle starts to appear. For temperatures above 130 °C, the semicircle is now fully resolved. Water evaporation effect in wet and dry samples is clearly identified when comparing the wide difference in the resistance value at 70 °C in dry annealed and wet samples as it is shown in Figure 2.9a and b. For dry annealed chitin (Fig. 2.9b), resistance drastically decreases as temperature increases, and the opposite behavior is present in wet samples (Fig. 2.9a); it means that heat treatment allows unmasking the real electrical properties of dry annealed chitin present below 70 °C. For wet samples, water evaporation on heating increases chitin resistivity response; however, this trend changes above 70 °C once water has been removed and water effect vanishes.

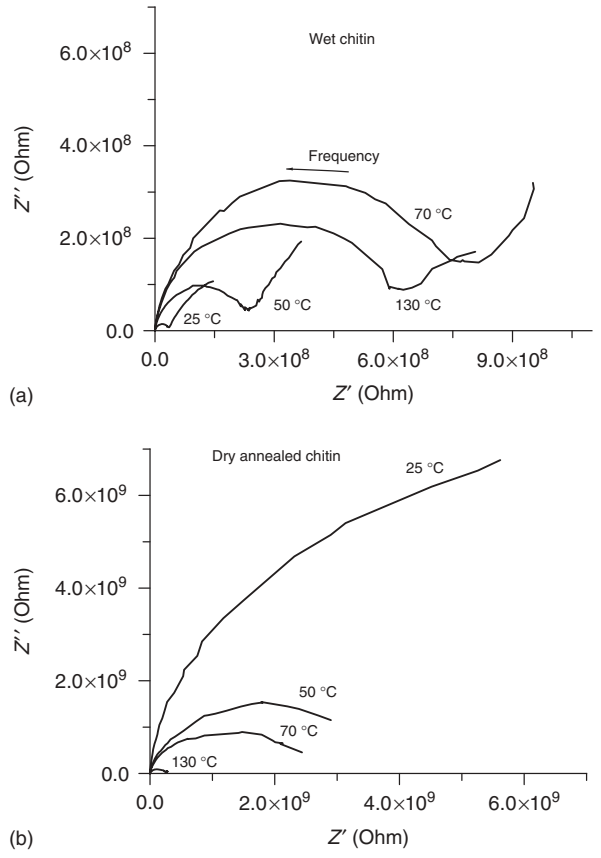

Figure 2.9 Complex dielectric spectrums of wet and dry annealed chitin films. Note the strong free water effect: for wet samples, resistance increases as temperature increases. An opposite effect is observed in dry annealed samples. *Source*: Reproduced with permission from González-Campos JB, Prokhorov E, Luna-Bárcenas G, Mendoza-Galván A, Sanchez IC, Nuño-Donlucas SM, García-Gaitan B, Kovalenko Y. J Polym Sci B Polym Phys 2009;47:932 [5]. Copyright 2009 John Wiley and Sons, Inc.

The same dielectric behavior in dry annealed and wet samples is developed above 110 °C. These observations are very important since they suggest an extra relaxation process [16] in the absence of water, which is analyzed in detail in the next section. On the other hand, the linear response at low frequencies in wet and dry chitin can be associated with interfacial polarization in the bulk films and/or surface and metal contact effects [47]. To analyze the dielectric relaxation of chitin films is necessary to understand the nature of the low frequency part of dielectric spectrum.

2.7.3.1 Electrode and Interfacial Polarization Effects

It is well known that contact metal–polymers for many systems can be interpreted as Schottky barriers [55–57] or heterojunction [58, 59]. To test the influence of gold contact on the chitin dielectric spectra, a nonsymmetrical contact array was prepared in the following manner: a circular chitin film was covered on one side with a piece of gold sheet with a small circular orifice in the center during gold-sputtering. The other side of the film was totally gold-sputtered. This way a top surface available for electrode contact is circa 0.008 cm^2. The bottom surface area is circa 0.75 cm^2. Because of contact surface area differences, the current depends on the properties of the top electrode.

Figure 2.10 shows dielectric measurements on wet chitin sample with different applied bias voltage at 23 and 50 °C. The bias increase leads to a reduction of barrier resistance that changes the low frequency contribution of dielectric spectra (which occur at large values of Z'). As can be seen, a deviation from a semicircle is seen at both temperatures, and the response depends on the bias voltage. These data are a good indication of contact polarization effects related to the (partial) blocking of charge carriers at the sample/electrode interface [60]. This low frequency part of the electrical response is easily influenced by imperfect contact between the metal electrode and the sample. In fitting dielectric data to models, this low frequency data needs to be discarded.

In addition to this electrode polarization, interfacial polarization effects are observed in the high temperature range (>170 °C) for all chitin films. This effect manifests as a "bulge" on the semicircle. Figure 2.10 illustrates this

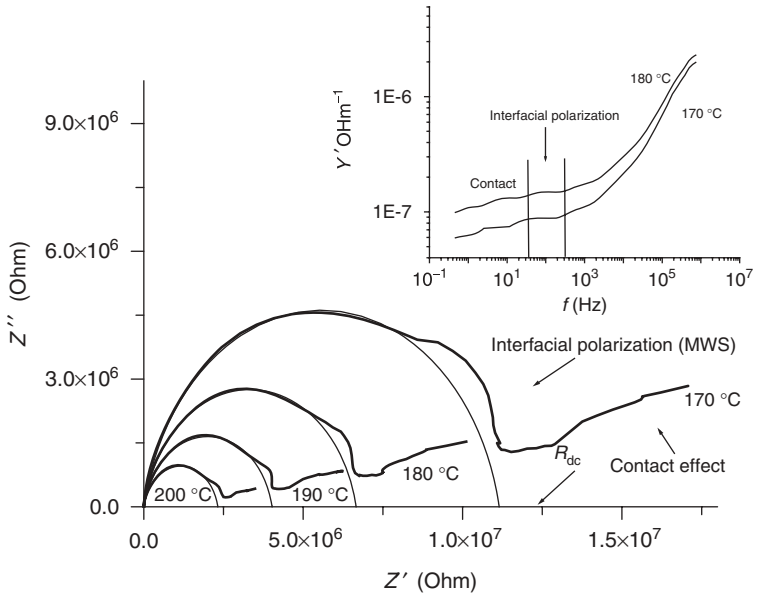

Figure 2.10 Dielectric spectra of chitin films with Maxwell–Wagner (MW) polarization at low frequency and high temperature. Interfacial polarization can be detected by the appearance of an extra semicircle. *Source*: Reproduced with permission from González-Campos JB, Prokhorov E, Luna-Bárcenas G, Mendoza-Galván A, Sanchez IC, Nuño-Donlucas SM, García-Gaitan B, Kovalenko Y. J Polym Sci B Polym Phys 2009;47:932 [5]. Copyright 2009 John Wiley and Sons, Inc.

effect at 170, 180, 190, and 200 °C. This is a common form of a discontinuity occurring in an inhomogeneous solid dielectric associated with internal interfaces; it is well known as the Maxwell–Wagner–Sillars (MWS) relaxation. The simplest model to describe interfacial polarization is the MWS double-layer model where each layer is characterized by its permittivity and conductivity. An equivalent circuit for interfacial polarization is constructed of two RC elements in series [9]. In polysaccharides [20] and biopolymers [21], the interfacial polarization (MWS polarization) was observed in low frequency and high temperature ranges. According to the classical model, the appearance of the interfacial polarization in dielectric spectrum can be observed as appearance of additional semicircle [41].

In the low frequency range, both contact and interfacial polarizations were observed in all samples. These polarizations have to be carefully considered; it is important to take into account only the so-called depressed semicircle that does not include contact and interfacial polarization effects.

Another critical issue is depicted in the inset of Figure 2.9. For most polysaccharides, a commonly used plot of admittance versus frequency does not reveal the appearance of the extra semicircle related to interfacial polarization. It is noteworthy that data treatment proposed in this study allows one to identify and separate these two processes (contact and interfacial polarization effects). A model-based analysis can be misleading if appropriate contact and interfacial polarizations are not considered.

2.7.3.2 dc Conductivity Correction A correction must be applied to all samples (specially the wet ones) since they exhibit a large conductivity contribution in the low frequency range. This dc conductivity strongly modifies the dielectric loss factor ε'' on the low frequency side (see Fig. 2.10 at 80 °C) where dielectric effects are completely masked. In this case, the ε'' can be expressed with Equation 2.2.

Commonly, ac conductivity is measured in the low frequency range where a plateau is expected to appear [20]. However, in our samples, this plateau is not resolved, as a consequence polarization and contact effects cannot be discerned and the correct dc conductivity cannot be calculated by this method (see inset in Fig. 2.10). To circumvent this problem, the alternative procedure described in Section 2.5.5 can be used.

2.7.3.3 Dielectric Relaxations Analysis Figure 2.11 shows the permittivity loss coefficient (ε'') data for dry annealed chitin before (80 °C, solid triangles) and after dc conductivity correction (open triangles). From dielectric measurements the frequencies at which contact/polarization effects become relevant (about 2 Hz for the contact effects

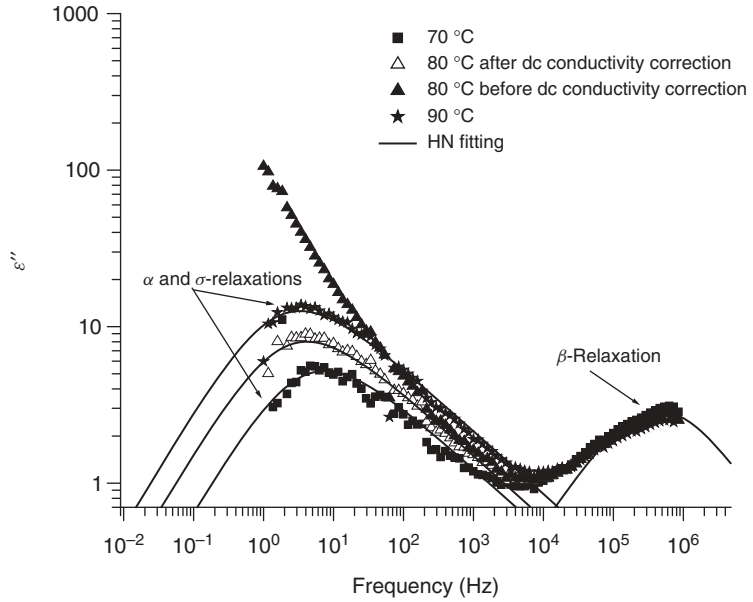

Figure 2.11 Loss coefficient curve (ε'') versus log frequency. *Source*: Reproduced with permission from González-Campos JB, Prokhorov E, Luna-Bárcenas G, Mendoza-Galván A, Sanchez IC, Nuño-Donlucas SM, García-Gaitan B, Kovalenko Y. J Polym Sci B Polym Phys 2009;47:932 [5]. Copyright 2009 John Wiley and Sons, Inc.

and about 100–300 Hz for polarization effects at the temperatures higher than 170 °C) have been estimated and are not considered for further analysis; above 80 °C a low frequency relaxation with Arrhenius temperature dependence (as will be shown later) is revealed, and below 80 °C a different relaxation with a non-Arrhenius temperature dependence that we designate as the primary or α-relaxation is disclosed. A similar behavior is seen at lower temperatures (not illustrated). Also notice in Figure 2.11 that the well-known β-relaxation found in β-chitin and CS [20, 21] is present on the high frequency side of the spectrum.

The activation plot of relaxation time for the non-Arrhenius dependence present in the low frequency range below 80 °C (Fig. 2.11) was obtained using the empirical HN [20]. For secondary relaxations with Arrhenius behavior, we used the Cole–Cole simple model [9] to obtain the activation plot for relaxation time. Some authors [21, 61] have used the model of HN to describe relaxations in polysaccharides. However, this requires more adjustable parameters. On the other hand, several authors have shown that these secondary relaxations are well described by the simpler Cole–Cole model (HN model with $\beta = 1$); this model has been successfully applied for the fitting of lateral group motions representing the β-relaxation [18, 62–64] and for describing the motion of ions ascribed to the α-relaxation [65].

For β-chitin as well as for various cellulose-based materials, starches, and nonpolymeric glass forming liquids, it was found that the activation energies from the dc conductivity plot and the dielectric α- and β-relaxation times (or α-peak frequency) are well correlated [66–68]. In glass-forming liquids, at high temperatures, both dc conductivity and relaxation time show an Arrhenius behavior with the same activation energy. Below a cross over temperature (T_c), a VFTH behavior was observed [68].

The two different temperature dependencies described above for glass-forming liquids are present in α-chitin, and the similarity between dc conductivity and relaxation time for the two low frequency relaxations is clearly observed in Figure 2.12a and b. Both dependencies (dc conductivity (σ_{dc}) and relaxation time (τ) versus $1/T$ plots) show the same features: an Arrhenius type relaxation will yield a straight line above 80 °C, whereas a non-Arrhenius relaxation will manifest as a curved line that suggests a VFTH type or glass transition below 80 °C in dry annealed samples. For wet and dry samples, the decrease of conductivity as the temperature is increased from 20 to 80 °C is likely due to the motion of water–polymer complex since water could be modifying the relaxation mechanism of the matrix material.

At higher temperatures, a thermally activated behavior similar to that of dry annealed chitin is recovered. For all chitin samples, the dc conductivity decreases and relaxation time increases (see Fig. 2.12a and compare with Fig. 2.12b) as temperature increases until circa 210 °C. This temperature signals polymer degradation; in agreement with thermogravimetric analysis in Figure 2.5, the onset of degradation is about 210 °C. Nonreversible degradation

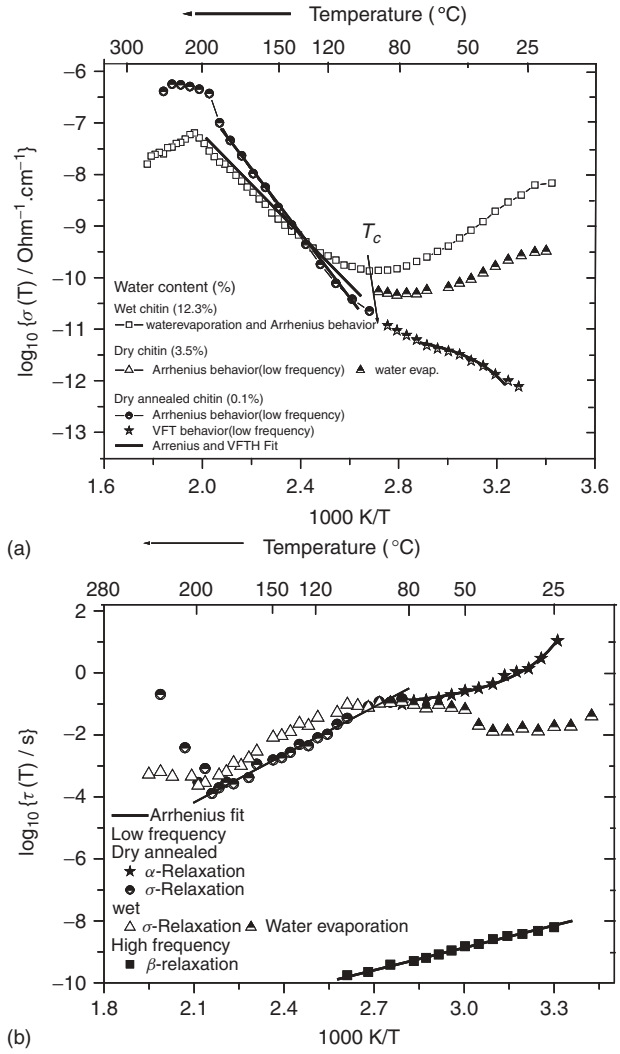

Figure 2.12 (a) Low frequency dc conductivity dependence with reciprocal temperature $1/T$ for wet and dry annealed α-chitin. (b) Relaxation time dependence versus $1/T$ at low frequency. *Source*: Reproduced with permission from González-Campos JB, Prokhorov E, Luna-Bárcenas G, Mendoza-Galván A, Sanchez IC, Nuño-Donlucas SM, García-Gaitan B, Kovalenko Y. J Polym Sci B Polym Phys 2009;47:932 [5]. Copyright 2009 John Wiley and Sons, Inc.

at high temperatures ($T > 210\,^{\circ}$C) is common to many polymers and polymer blends [69, 70].

Low Frequency Relaxations

THE LOW TEMPERATURE RELAXATION Although three different sample types are illustrated in Figure 2.12a and b (wet, dry, and dry annealed), let us focus on the dry annealed sample containing minimal moisture (∼0.1%). Above 80 °C, the temperature dependence is linear (Arrhenius), whereas below 80 °C it is non-Arrhenius. This shows that in this low frequency range (0.1 Hz to 1 MHz) a transition between two dynamical regions occurs at a crossover temperature (T_c) of ∼80 °C. This crossover temperature, discussed by Ferrari et al. [71], separates a cooperative motional process that obeys the VFT equation from an activated process, described by Arrhenius equation. It can also be considered as the temperature where cooperative motion of the α-relaxation sets in [68]. Schönhals et al. [72] as well as Cutroni et al. [68] showed similar behavior for glycerol and propylene glycol.

For most polymers, the relationship between the glass transition temperature T_g and T_0 is $T_g = T_0 + C$ where C is a constant that in many dielectric studies is about 50 K [9, 73, 74]. On the basis of the usual uncertainty in C and the above $T_0 = 285\ K$, we estimate that T_g for dry annealed chitin is $62 \pm 10\,^{\circ}$C. This low value for the T_g of a stiff polymer such as α-chitin is slightly surprising, but it is consistent with the low T_g's found in polypeptides (−70 to −50 °C) [75–77]. The common denominator between polysaccharides and polypeptides is extensive hydrogen bonding; significant thermal disruption of H-bonding and the onset of main chain molecular motions are probably closely related.

HIGH TEMPERATURE RELAXATION Even though the α-relaxation in amorphous polymers exhibits the typical VFT behavior in the whole temperature range above T_g, this is not the case for β-chitin and other hydrogen bonding polymers such as polypeptides [75]. In polysaccharides, there is another mechanism that intervenes and can mask the α-relaxation or glass transition. This activated process agrees very well with the σ-relaxation, which according to Reference 20 is thought to be associated with proton mobility. From the slope of the conductivity plot and relaxation time calculated with the Cole–Cole empirical model (HN equation with $\beta = 1$), it can be seen that above 80 °C the commonly VFT behavior developed by the α-relaxation changes to Arrhenius behavior to the onset of degradation. The activation energy for this σ-relaxation is calculated to be 113 ± 3 kJ/mol for dry annealed chitin and 89 ± 1 kJ/mol in wet samples. These values agree with those reported for other polysaccharides (95–110 kJ/mol) [66] in the high temperature range (>80 °C) (Table 2.1) and the closely related CS [21].

High Frequency Relaxation As illustrated in Figure 2.11, in dry annealed chitin samples, a high frequency secondary relaxation is observed, the so-called β-relaxation. This relaxation is found in other polysaccharides [66] and is thought to be associated with molecular motions via the glucosidic bond [20, 61]. The fitting parameter $\alpha = 0.45 - 0.49 \pm 0.08$ and the intensity of β-relaxation have a weak dependence on temperature. $\beta = 1$ values in the HN model describe a symmetric relaxation by the simple Cole–Cole model. It can be seen

TABLE 2.1 Parameter Values for the Arrhenius-Type Dependence in σ-Relaxation from dc Conductivity and Relaxation Time. Low Frequency Relaxation in the 80–210 °C Range

Sample	Conductivity Relaxation Time			
	$E_{a\sigma}$	σ_0(S cm^{-1})	$E_{a\tau}$ (kJ/mol)	τ_0(s)
Wet chitin (this study)	88.9 ± 1	79.8 ± 2.2	91.9 ± 4.4	$4.2 \pm 0.4 \times 10^{-15}$
Dry annealed chitin (this study)	113.2 ± 3	$1.32 \times 10^5 \pm 2.6$	110.7 ± 3.7	$7.76 \pm 0.3 \times 10^{-16}$
Polysaccharides Einfeldt et al. [20]	—	—	95–110	Not reported
Chitosan (dry annealed) Viciosa et al. [21]	—	—	94 ± 2	0.2×10^{-16}

TABLE 2.2 Arrhenius Parameters for the Secondary Relaxation Process Found at High Frequencies

	β-Relaxation	
	E_a (kJ/mol)	τ_0 (s)
Einfeldt et al. [20]		
β-Chitin	44.7	3.9×10^{-16}
Viciosa et al. [21]		
Chitosan	49.0 ± 1	$0.44 \pm 0.07 \times 10^{-16}$
This Study		
α-Chitin (dry annealed)	44.6 ± 0.9	1.33×10^{-16}

that the experimental data could be well fitted to the Cole–Cole model, involving less number of parameters in agreement with other authors [9, 62, 63]. The temperature dependence of the relaxation time is Arrhenius with activation energy of 45 ± 1 kJ/mol for dry annealed chitin (Table 2.2) in agreement with previous reports on β-chitin and CS [20, 21]. The same Arrhenius behavior is kept above and below the glass transition temperature.

2.7.4 Chitin Molecular Relaxations Conclusions

Impedance spectroscopy measurements have been used to investigate molecular dynamics in α-chitin. After dc conductivity correction, the exclusion of contact and interfacial polarization effects, and obtaining a condition of minimum moisture content (∼0.1%), the α-relaxation process that likely represents the glass transition is unveil.

The α-relaxation in dry annealed α-chitin can be observed by DS measurements. On this basis, the glass transition temperature was estimated at 61 ± 10 °C. Moisture content is a key factor to observed the glass transition in chitin and it could be related to the controversy about the glass transition temperature detection and designation in this biopolymer

The secondary β-relaxation is also observed in α-chitin from 80 °C to the onset of thermal degradation (∼210 °C). It exhibits a normal Arrhenius-type temperature dependence with activation energy of 113 ± 3 kJ/mol.

Finally, a high frequency secondary σ-relaxation is observed in dry annealed chitin with Arrhenius activation energy of 45 ± 1 kJ/mol comparable to that occurring in β-chitin, CS, and cellulose.

2.8 DIELECTRIC RELAXATIONS IN NEUTRALIZED AND NONNEUTRALIZED CHITOSAN: THE STRONGER WATER CONTENT EFFECT ON THE α-RELAXATION AND THE GLASS TRANSITION PHENOMENON

2.8.1 Low Frequency Relaxations: The Influence of Moisture Content on Dielectric Measurements

Once contact and interfacial polarization were discarded and dc corrections are carried out, high and low frequency relaxations are identified in CS films. Figure 2.13 shows the $\log_{10}$ conductivity versus $1/T$ dependence in the low (10^0–10^3 Hz) and high (10^3–10^6 Hz) frequency ranges. Both neutralized and nonneutralized films with different moisture contents show similar behavior; the nonneutralized CS films show higher conductivity values, which could indicate higher mobility and/or number of conducting species (NH_3^+ groups) [21]. Once again, these low frequency relaxations can be analyzed in two different temperature ranges: the nonlinear "low temperature relaxation" with the characteristic trend of the glass transition phenomenon present from 20 to 70 °C, and the Arrhenius-type "high temperature relaxation" from 70 °C to the onset of degradation ∼210 °C.

2.8.1.1 Low Temperature Relaxation The low temperature relaxation is highly influenced by moisture content; in wet samples, the conductivity decreases as water evaporates, disguising the actual dielectric properties of CS above 100 °C, while for moisture contents lower than 3 wt% and higher than 0.5 wt% (dry films), a non-Arrhenius behavior appears. However, in dry annealed CS (moisture contents <0.05 wt%), this low temperature relaxation vanishes after the second heat treatment.

As in chitin, the $\log_{10}$ conductivity versus $1/T$ also shows the nonlinear behavior developed in dry samples. This nonlinear dependence is the typical trend of the

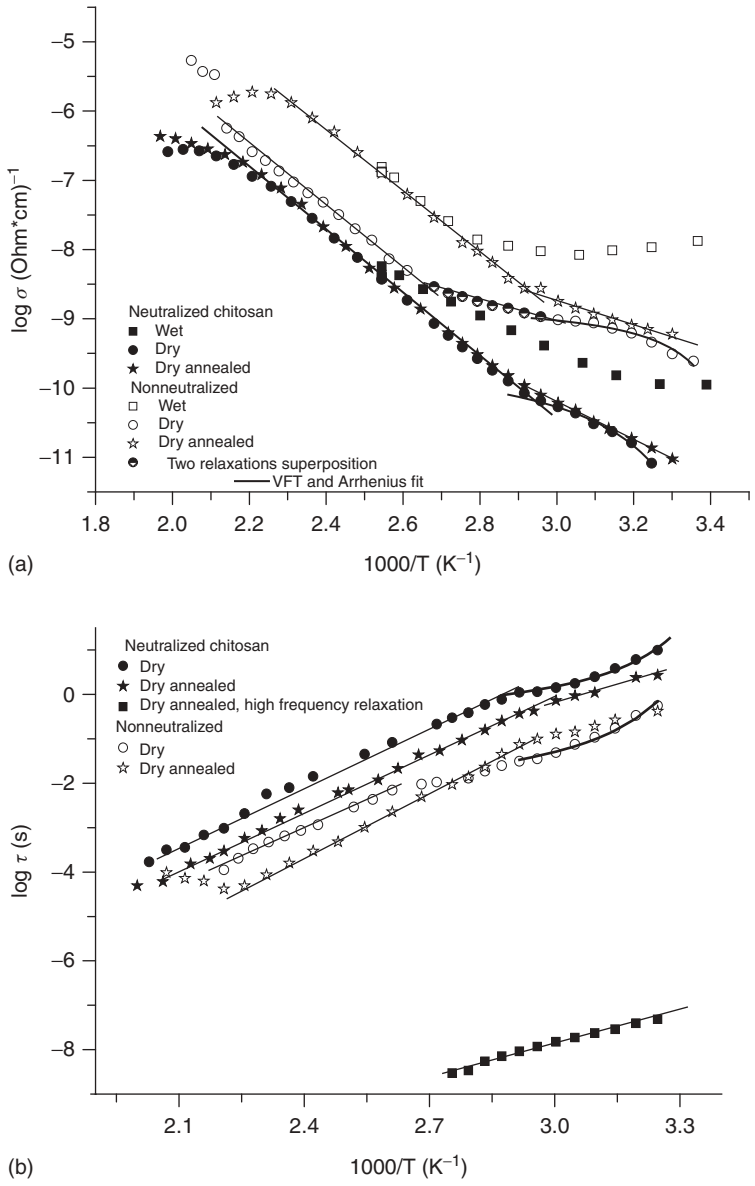

Figure 2.13 (a) $\log_{10}\ \sigma$ versus $1/T$ for wet, dry, and dry annealed chitosan (neutralized and nonneutralized). (b) $\log_{10}$ relaxation time versus $1/T$. *Source*: Reproduced with permission from González-Campos JB, Prokhorov E, Luna-Bárcenas G, Fonseca-García A, Sanchez IC. J Polym Sci B Polym Phys 2009;47:2259 [6]. Copyright 2009 John Wiley and Sons, Inc.

α-relaxation behavior related to the dynamic glass transition [9, 37]. The temperature dependence of conductivity and relaxation time calculated are well described by the VFTH equation [9]. There is an excellent agreement between the Vogel temperature calculated by conductivity and relaxation time independently ($T_0 = 284$ K in both cases). Note that nonneutralized films exhibit higher conductivity than the neutralized ones, which is consistent with the excess number of protons in the nonneutralized films (NH_3^+ groups are present). In addition, the T_0 value is independent of the presence of NH_3^+ groups. With this T_0 value, a T_g value can be estimated for neutralized and nonneutralized CS of 61 °C.

A strong effect of moisture content on the VFT behavior describing the α-relaxation process is evidenced in Figure 2.14, since for dry samples the glass transition temperature shifts to higher values as moisture content decreases. It is possible to identify this effect when different annealing temperatures (Fig. 2.13) are used during measurements on the same sample. This shifting of the glass transition temperature to higher values for lower moisture contents suggests a plasticizing effect of water

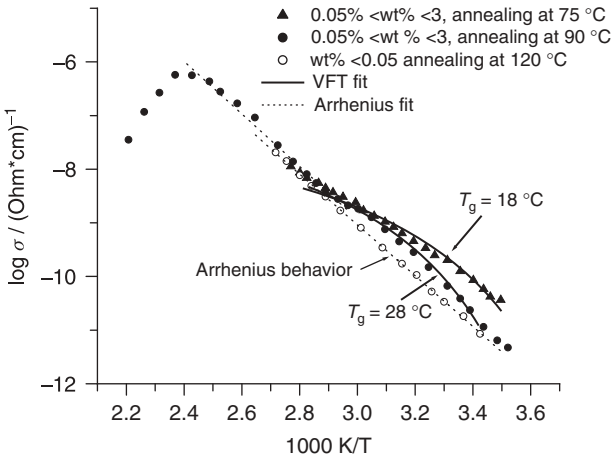

Figure 2.14 $\log_{10}$ conductivity versus $1/T$ for nonneutralized chitosan. *Source*: Reproduced with permission from González-Campos JB, Prokhorov E, Luna-Bárcenas G, Fonseca-García A, Sanchez IC. J Polym Sci B Polym Phys 2009;47:2259 [6]. Copyright 2009 John Wiley and Sons, Inc.

on CS glass transition. In our case, the accurate moisture content in the 0.05–3 wt% range according to the annealing treatment at different temperatures is difficult to determine since all the measurements are performed in a vacuum cell. However, it is noteworthy that moisture contents between 0.05 and 3 wt% are needed to distinguish the α-relaxation process by dielectric measurements before it vanishes at 0.05 wt% moisture content with the 120 °C annealing treatment (Figs 2.13a and b, and 2.14).

As mentioned before, there exists a great controversy about the glass transition temperature (T_g) of CS; some authors show no evidence of a glass transition by DSC, DMTA, and dielectric measurements [19–21], while others report a wide variety of values. Sakurai et al. [18] assigned a T_g of 203 °C in nonneutralized films by DSC and DMTA techniques; however, our TGA, DSC (Figs 2.5 and 2.6), and dielectric measurements show that this value is very close to chemical degradation. Additionally, to eliminate the effect of moisture, Sakurai et al. [18] performed two cycles of heating and cooling runs by heating up to 180 °C; however, as previously explained, degradation of CS starts at 170 °C. Liu et al. assigned a T_g of 91.8 °C [17]. It is not clear if their DSC measurements come from the first or second scan; this result seems to correspond to water elimination rather than a glass transition.

Lazaridou et al. [78] estimated a T_g ∼95 °C, by DMTA measurements, for dry CS through the relationship between T_g and moisture in samples with an empirical equation. Using the same technique, Toffey et al. [79] determined a T_g = 82 °C for CS acetate. Quijada-Garrido et al. [80] by DSC measurements found no glass transition evidence; however, by DMTA they assigned ∼85–90 °C (depending on frequency). Mucha et al. [16] reported an α-relaxation assigned by DMTA measurements in the 156–170 °C range and by DSC in the range of 170–180 °C. They also found other molecular relaxation at 43 °C, which lies in the temperature range proposed in the present work. However, Mucha et al. [16] relate this molecular event to reorganization of packing of CS molecules due to an increase of residual water mobility, volume expansion, and following a change of hydrogen bond strength. Dong et al. [4] by four different techniques (including DMTA) assigned 140–150 °C as the glass transition temperature of CS. Kaymin et al. [81], using linear dilatometry and thermomechanical analysis, stated 55 °C as the glass transition temperature, which is very close to the result presented in this work.

CS has functional groups such as hydroxyls, amines, and amides, which can act as hydrogen bond acceptors or donors. For this reason, CS can be bonded or linked with hydrogen bond donors or acceptor compounds like water [80]. In the case of glass transition temperature, plasticization occurs only in the amorphous region, such that the degree of hydration is quoted as moisture content in the amorphous region [82]. As reported in the literature review, in these biopolymers, water can be present in three states: (i) nonfreezing water, (ii) freezable bond water, and (iii) free water [38, 80, 66]. According to Reference 83, the water sorption mechanism is composed of two main steps: water sorption on polymer sites and water clustering surrounding the first absorbed water molecules.

The α-relaxation process is strongly affected by the moisture content in the films as shown in Fig. 2.13a and b. While at percentages higher than 3 wt%, this process cannot be distinguished because of the free water effect, at lower percents (<3 wt% freezable bond water) a glass transition temperature can be assigned by the motion of a water–polymer complex in amorphous regions; a glass transition temperature can be assigned depending upon moisture content limited to be between 0.05 and 3 wt%. According to Reference 80, the glass transition must be interpreted as torsional oscillations between two glucosamine rings across glucosidic oxygens and a cooperative hydrogen bonds reordering. Water sorption in hydrophilic polymers is usually a nonideal process leading to plasticization [83]. Water leads to an increase in the amounts of hydrogen bonds producing an increase in cooperative motion. Water hydrogen bonds between CS chains and increases free volume. When this happens, chains can slide past each other more easily, and so the time scale of the cooperative motion matches that of the experiment and the glass transition can be detected.

If sample moisture is minimized (<0.05 wt%), chains are able to interact with each other giving rise to a denser packing. Thereby, the mobility of polymer chains decreases and the glass transition phenomenon is not easily detected.

Because of the absence of water, the glass transition temperature could shift to temperatures above 70 °C (more rigid backbone). Ogura et al. [84] report by DMA analyses that chitin and CS's dynamic mechanical properties of wet films were greatly affected by the presence of water. For chitin, they observed a loss peak at 50 °C and it was attributed it to the glass transition of chitin plasticized with water. Regarding dry CS films, a glass transition was assigned at circa 140 °C [82]. However, these results are not theoretically connected to a glass transition, and so it is difficult to assign the observations to a specific molecular relaxation.

When water is minimized (0.05 wt% of water, Fig. 2.13a) and plasticization is absent, the glass transition temperature could shift to higher temperatures. At this point (above 70 °C), another molecular relaxation takes place and the α-relaxation is weaker and cannot be observed because of the high temperature relaxation effect; this is clearly observed in dry annealed CS below 70 °C (Fig. 2.13a and b) by a change of the VFT behavior to a linear one with a different slope than that for the high temperature process. This "new" slope is a behavior halfway between the nonlinear VFT behavior and the Arrhenius high temperature one, since under certain conditions of minimum moisture, the high temperature relaxation process is observed in the whole temperature range before the onset of thermal degradation as shown in Figure 2.14.

The controversy and particularly the discrepancy in the glass transition temperature of CS can be related to an inefficient elimination of water, a heat treatment near the degradation temperature of CS, the film preparation technique, neutralization process, or even deacetilation degree (%DD) (even though Dong et al. [4] showed no %DD influence on T_g value, Maria Mucha et al. [16] found the opposite). But without doubt, the moisture content determines whether the glass transition temperature in CS can be observed. As it can be seen, the presence of water drastically affects the CS backbone mobility, especially in the α-relaxation region that corresponds to the cooperative motion. Moisture content is probably the main cause of the wide glass transition temperatures range reported in literature.

2.8.1.2 High Temperature Relaxation The "high temperature" relaxation arises at 80 °C until the onset of degradation ~210 °C (Figs. 2.13a and b). It can be well described by the Arrhenius model and is present in both neutralized and nonneutralized CS. The slope of these curve represent the activation energy of each process. The temperature dependence of dc conductivity and relaxation time are Arrhenius type. For this relaxation, nonneutralized CS films seem to be more sensitive to water, since in the dry state presents a particular behavior in the 70–100 °C temperature range, which is recognized as a superposition of two relaxation processes, giving raise a different slope value.

The shape of this relaxation seems to be symmetric; the HN fitting parameters [9] $\alpha = 0.72 \pm 0.08$ and $\beta = 1.0 \pm 0.09$ are temperature independent in both CS forms, in agreement with previous studies [20]. A value of $\beta = 1$ describes a symmetric relaxations that can be described by the simpler Cole–Cole model. It can be seen that the experimental data could be fitted with the Cole–Cole model involving less parameters in agreement with other authors [62, 65].

Activation energy calculations are in agreement with previous reports for neutralized and nonneutralized CS [21, 5] and for polysaccharides [20]. The activation energy values for both films are quite close. Einfeldt et al. [20] observed this relaxation process in the high temperature range (>80 °C); however, on minimum moisture conditions (Figs 2.13 and 2.14), this relaxation process discloses in the whole temperature range until the onset of thermal degradation. This process, the so-called σ-relaxation, has been widely studied and is associated with the hopping motion of ions in the disordered structure of the biomaterial [20].

For the case of nonneutralized films, moisture has a strong effect on the σ-relaxation. This is shown in the dry nonneutralized samples in the 70–100 °C temperature range with moisture content in the range of 0.05–3.5 wt% (Figs 2.13a and 2.14). Note that a lower slope (lower activation energy) ascribed to the superposition of α- and σ-relaxations (as explained above) describes this "new" Arrhenius-type σ-relaxation for nonneutralized films. Activation energy is circa $E_{a\sigma}$ (conductivity) $\approx$ 28.8 and $E_{a\tau}$ (time relaxation) $\approx$ 38.34 kJ/mol, which is much smaller than that of neutralized films with similar moisture content (~80–85 kJ/mol; Table 2.2). The activation energy value of the relaxation time for the σ-relaxation process in the dry samples shows that water exerts a greater effect on the nonneutralized CS form; this is because of its superior ability to form hydrogen bonds providing a lower activation barrier for motion of ions. In this CS form, the σ-relaxation process is shifted to slightly higher frequencies compared to neutralized CS as shown in Figure 2.15. This implies lower relaxation times (Fig. 2.13b) and lower pre-exponential factor values (Table 2.1). As mentioned before, the nonneutralized films possesses higher conductivity conferred by NH_3^+ groups, and so ion mobility in nonneutralized CS is facilitated than in neutralized samples. Solid lines represent the HN fitting; it is in excellent agreement with the experimental results.

Pizzoli et al. [85] by DMA and dielectric measurements observed a "high temperature relaxation" near 140 °C; the calculated activation energy was ~100 kJ/mol, and this value is in agreement with the activation energy of the

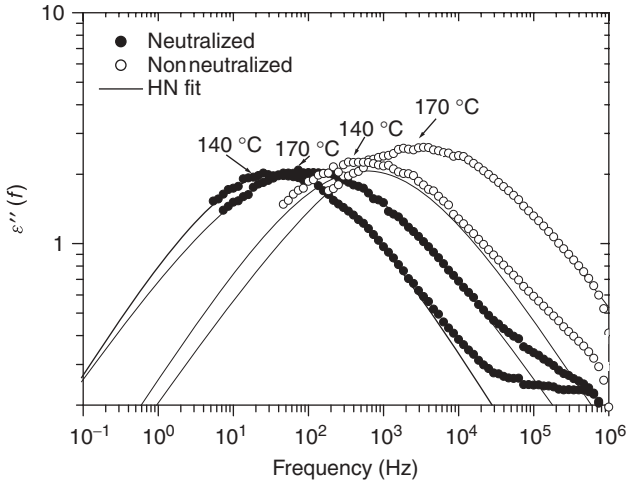

Figure 2.15 Loss factor (ε'') versus frequency. σ-Relaxation process shifts to higher frequencies with temperature for nonneutralized chitosan. *Source*: Reproduced with permission from González-Campos JB, Prokhorov E, Luna-Bárcenas G, Fonseca-García A, Sanchez IC. J Polym Sci B Polym Phys 2009;47:2259 [6]. Copyright 2009 John Wiley and Sons, Inc.

σ-relaxation mentioned before. They did not interpret it as a glass transition and suggested that this relaxation arises from a molecular motion having a less cooperative character than the glass-to-rubber transition. Some authors have attributed this relaxation to the glass transition [4, 16]; nonetheless, it seems to be ion motion that yields this peak in dynamic mechanical spectra and not the glass transition, because the activation energy for segmental mobility should be greater.

A change from positive slope in the conductivity (Fig. 2.13a) to negative in the relaxation time (Fig. 2.13b) plots is present at 210 °C and above; it denotes the onset of degradation, at this temperature the dependence of resistance and capacitance versus temperature also experiment a change in the slope (not shown). TGA and DSC (not shown) measurements confirm this degradation.

The large decreases of the electrical conductivity, which have been observed for all those materials, correspond to an irreversible chemical degradation of the polymer film. During heating, CS films change color from white to brown at temperatures above 200 °C. This effect has also been reported for fibrous CS [86], which changed color from white to pale yellow at 140 °C and to yellowish brown at 160 °C. DSC and TGA analyses have shown that CS's thermal degradation starts about 170 °C [87, 88].

2.8.2 High Frequency Relaxation

In the high frequency region (104–108 Hz) for dry and dry annealed neutralized and nonneutralized CS, a secondary relaxation process is identified as β-relaxation. In wet (11% moisture content) samples, this relaxation is not well resolved and model-fitting is complicated. This is the reason we cannot identify the β_{wet} relaxation process documented by other authors attributed to motion due to biopolymer-swollen water [85, 88]. For wet polysaccharides, Enfieldt et al. [20] reported a superposition of two relaxation processes: β- and β_{wet} relaxations that merge into one common β-relaxation process as water is driven off.

The temperature dependence of the relaxation time for this high frequency relaxation is found to be Arrhenius type; this behavior is shown in Figure 2.13b. Note an excellent linear fitting of the relaxation time as a function of $1/T$. Table 2.3 lists the parameter values obtained for this process in both CS samples.

These activation energy values are in excellent agreement with previous reports enlisted in Table 4.6. This β-relaxation is the most commonly reported relaxation process in CS [20, 21]; it has been related to side group motions by means of the glucosidic linkage [20, 79]. β-Relaxation is the main relaxation process found in all pure polysaccharides in the low temperature range (−135 to +20 °C) and corresponds to local chain dynamics [20]. For CS, we have found this secondary relaxation in the high temperature range in agreement with other authors (higher than 20 °C) [20, 61]; however, it is expected to appear in the high temperature range at the very high frequency end as Einfeldt et al. [20] stated. They found this high frequency relaxation at temperatures as high as 120 °C.

2.8.3 Chitosan Molecular Relaxations: Conclusions

The molecular dynamics of neutralized and nonneutralized CS was studied by DS and DMA. The low frequency α-relaxation associated with the glass transition can be clearly observed by DS. This relaxation process seems

TABLE 2.3 Arrhenius Parameters for the Secondary Relaxation Process Found at High Frequencies

	β-Relaxation	
	$E_{a\tau}$ (kJ/mol)	τ_0(s)
Dry Chitosan (This Study)		
Neutralized	46.0 ± 1.3	$(8.2 \pm 1.6) \times 10^{-16}$
Nonneutralized	46.0 ± 1.3	$(1.9 \pm 0.5) \times 10^{-15}$
Dry Annealed Chitosan (This Study)		
Neutralized	48.5 ± 1.8	$(6.3 \pm 1.9) \times 10^{-17}$
Nonneutralized	46.7 ± 0.4	$(6.4 \pm 1.1) \times 10^{-15}$
Viciosa et al. [61]		
Neutralized	46 ± 2	$(5.1 \pm 2.4) \times 10^{-16}$
Nonneutralized	47 ± 1	$(3.4 \pm 1.6) \times 10^{-16}$
Einfeldt et al. [20]		
β-Chitin (dry annealed)	44.7	3.9×10^{-16}
Chitosan	47.8	0.8×10^{-16}

to be independent of the CS form evaluated (neutralized and nonneutralized) and is strongly influenced by moisture content; a glass transition can be calculated depending upon moisture content.

A plasticizing effect on CS α-relaxation is observed by DS. For moisture contents less than 0.05 wt%, the glass transition is difficult to observe due to the superposition of two relaxation process.

Impedance spectroscopy is a powerful tool to monitor the plasticizing effect of water on CS glass transition.

The well-known secondary σ-relaxation often associated with proton mobility is also observed in CS (neutralized and nonneutralized) from 80 °C to the onset of degradation. On minimum moisture content conditions, this relaxation process could be noticed in the whole temperature range before the onset of thermal degradation. It is strongly affected by moisture content for dry samples; by water effects, the activation energy shifts to lower values when compared to dry annealed samples. The nonneutralized CS showed an easier mobility in this ion motion process. This relaxation process exhibits a normal Arrhenius-type temperature dependence with activation energy of 80–90 kJ/mol.

Finally, the high frequency secondary β-relaxation is also observed with Arrhenius activation energy of 46–48 kJ/mol.

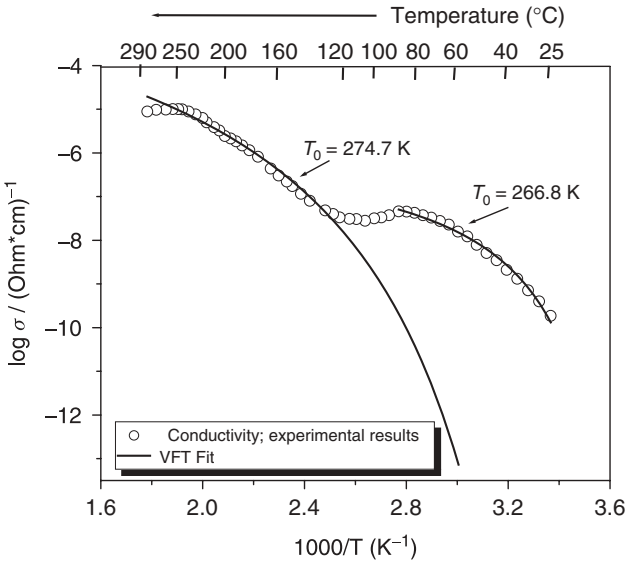

Figure 2.16 dc Conductivity (σ_{dc}) as a function of 1000/*T* PVA II. Note: two different regions with VFT behavior are observed. *Source*: Reproduced with permission from González-Campos JB, García-Carvajal ZY, Prokhorov E, Luna-Bárcenas JG, Mendoza-Duarte ME, Lara-Romero J, Del Río RE, Sanchez IC. J Appl Polym Sci 2012;125:4082 [7]. Copyright 2012 John Wiley and Sons, Inc.

2.9 PVA DIELECTRIC RELAXATIONS

Figure 2.16 shows the change in dc conductivity as a function of temperature from 25 to 300 °C for a wet PVA II film (only one scan with no annealing treatment). It can be seen that conductivity increases as temperature increases and this dependence unveils two well-defined regions at low and high temperatures, with an intermediate discontinuity between 80 and 140 °C that is associated with water evaporation. Both relaxation regions disclose a well-defined non-Arrhenius behavior usually observed in many glass-formers and well described by the well-known VFT related to the α-relaxation. This is a clear evidence of the glass transition phenomenon; however, this behavior is not disclosed in the whole temperature range.

As illustrated in Figure 2.16, two different Vogel temperatures (T_0) can be calculated by fitting the experimental data to the VFT model described above. The low temperature region (below 80 °C) displays a lower Vogel temperature than the high temperature region (above 130 °C), suggesting a plasticizing effect of water on PVA.

Figure 2.16 shows two regions: one from 25 to 80 °C and another one from 120 to 227 °C. A conductivity decrease is observed from 80 to 120 °C due to water evaporation, as noted above. It is noteworthy that these two different temperature regions have been previously described by Hanafy [30] for pure PVA and $GdCl_3$-doped PVA films. Hanafy [30] classified these two regions as region I from circa 30 to 60 °C and region II from circa 84 to 135 °C to propose two Arrhenius-type relaxations for pure PVA films. However, if we compare the data of Hanafy [30] with our study, one may argue the validity of the linear relationship (Arrhenius-type) of the conductivity with reciprocal temperature. When data are taken up to 300 °C (Fig. 2.16), a non-Arrhenius-type relationship is evidenced in both low (25–80 °C) and high (120–227 °C) temperature regions. This subtlety has been previously addressed by our group in polysaccharides and polysaccharides nanocomposites to resolve a non-Arrhenius-type versus an Arrhenius-type relaxation controversy [5–7].

In the above context, Bhargav et al. [89] reported a single Arrhenius behavior for the dependence of conductivity in the 30–100 °C temperature range for pure PVA, but their activation energy is almost two times higher than that of Hanafy [30]. On the other hand, Agrawal et al. [90] also suggested a VFT behavior of conductivity in pure PVA and PVA with ammonium salt films, but no further discussion is provided on the nature of the relaxations.

Figure 2.16 suggests that on heating a PVA film with moisture contents >3.5% are plasticized such that the first low temperature region (25–80 °C), described by VFT model, represents the depressed T_g of PVA circa 44 °C. As heating continues, water evaporates at 80–120 °C and the conductivity decreases. Further heating, after moisture

removal, produces an increase in conductivity up to 227 °C. At higher temperatures (227–300 °C) conductivity decreases denoting the onset of the melting point.

A VFT fitting in the high temperature region (120–227 °C) allows one to perform an extrapolation to lower temperatures. This extrapolation suggests a continuation of the primary relaxation in the high temperature that extends to lower temperatures circa 60 °C (see model extrapolation in Fig. 2.16). Under special sample conditions, the low temperature region will vanish, thus revealing a single VFT-type relaxation.

We now propose to perform dielectric measurements on samples of controlled moisture contents based on the above observations. Similarly, as those samples prepared for DSC and DMA analyses, we study samples PVA films annealed at 130 °C (water content <0.01% as calculated by TGA) and wet samples with moisture contents <3.5%. The results are shown in Figure 2.17.

Figure 2.17 shows that dry (annealed) PVA films only exhibit one VFT-type relaxation in the whole temperature range of our study and that the low temperature region vanishes (in wet samples). These results strongly suggest that the low temperature region in wet samples is related to the depressed T_g. The high temperature region (after moisture evaporation) is the VFT-type trace of dry PVA films. This is exactly shown in Figure 2.17 when comparing wet and dry (annealed) PVA films.

Calculations on VFT model show that Vogel temperatures for dry PVA is $T_0 = 267.2$ K; then, on the basis of the 50 K rule explained above, a T_g of 317.2 K = 44.0 °C can be now proposed from dielectric measurements for dry PVA.

By means of the imaginary part (Z″) impedance spectra, it is possible to get more details about the α-relaxation dependence on temperature and water content as shown in Figure 2.18a and b. For wet samples, it is possible to observe the α-peak in the low frequency side merely above 70 °C, and it is clear that the relaxation frequency increases with rise in temperature (Fig. 2.18a). Above 195 °C, a second relaxation related to crystalline PVA regions (melting) begins to appear in the low frequency side of the spectra, remaining the α-relaxation but now in the high frequency side. The α-peaks exhibited by the dry film shift to lower frequencies for temperatures below 100 °C (Fig. 2.18b), with an increase in magnitude compared to wet ones; this displacement is a clear signal about the masking effect of water on the real dielectric properties of PVA.

The relaxation time obtained for each temperature from the maximum of the imaginary part of the dielectric modulus (M^*), the M'' peak ($K = 1/2\pi f_{max}$) is shown in window inset of Figure 2.18a. Wet films display the trend akin to conductivity as temperature increases; two VFT behaviors in the high and low temperature range separated by water evaporation effect in the 80–140 °C temperature range. The T_0 calculated from the VFT model to the relaxation time data (Fig. 2.18) is in agreement with that obtained by the conductivity plot (Fig. 2.16). The observed T_g is commonly considered as the temperature

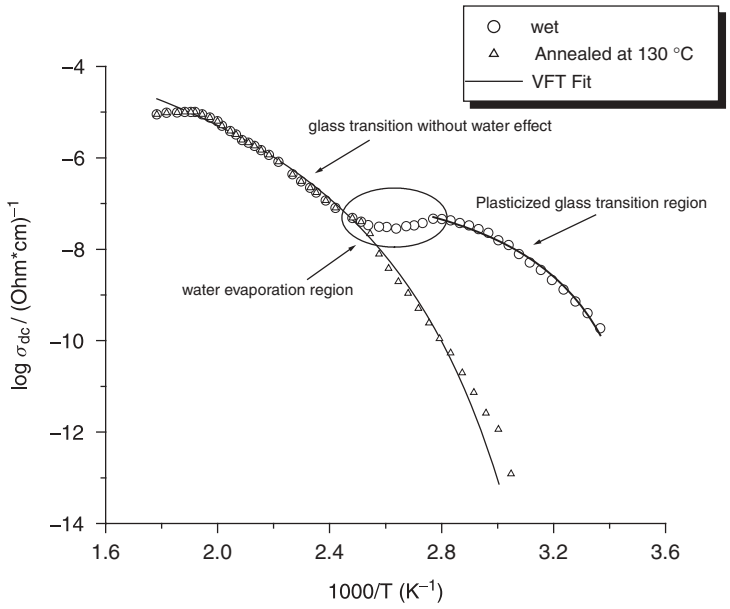

Figure 2.17 *log* σ_{dc} versus 1000/T for wet and dry PVA. Note: the VFT is extended in the whole temperature range after annealing at 130 °C, both low and high temperature regions merge into one. Window inset: 1000/T dependence of relaxation time (τ).

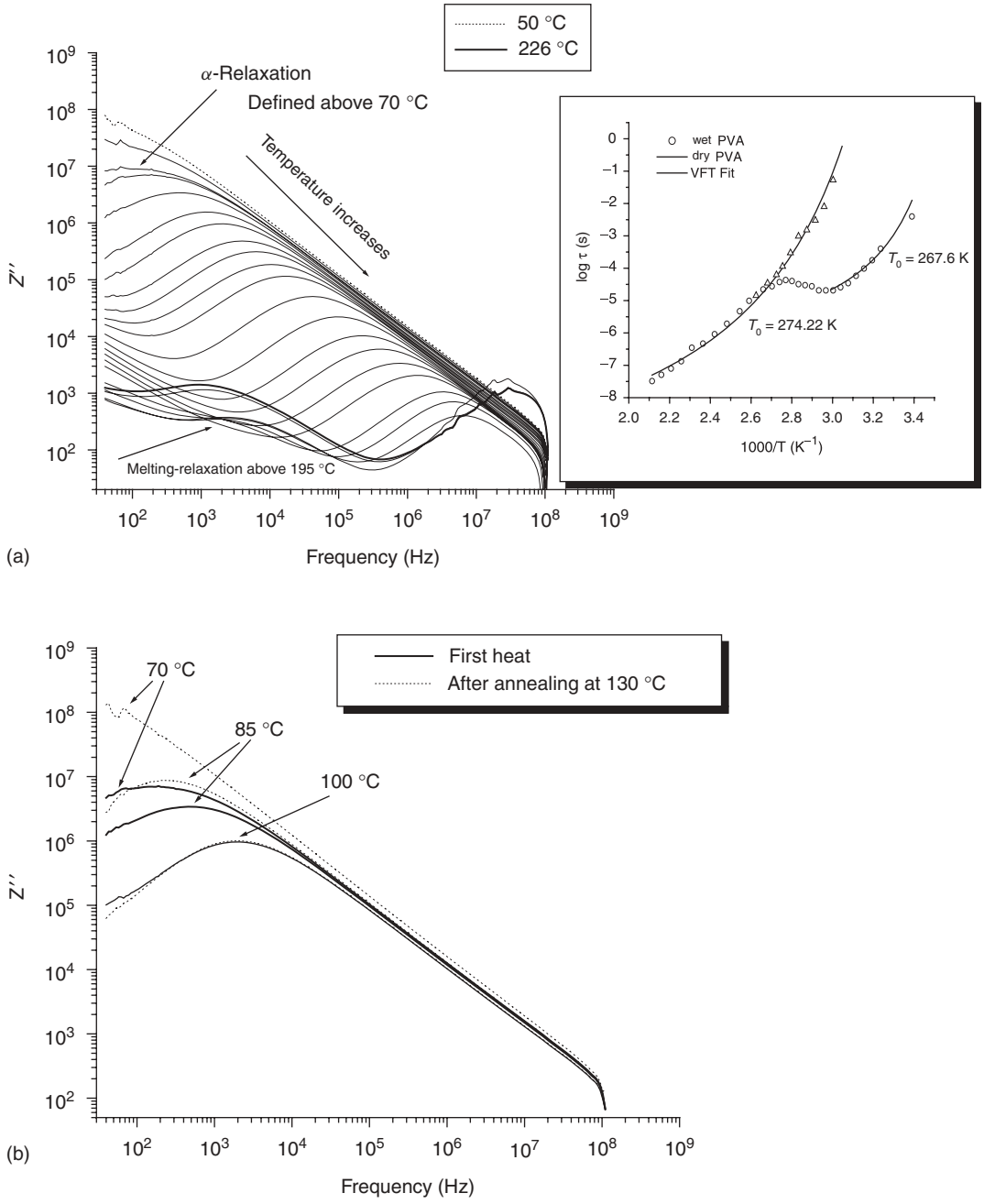

Figure 2.18 Impedance imaginary part (Z″) of the spectra versus frequency for (a) wet PVA and (b) wet and dry PVA. Note: α-Relaxation shifts to lower frequencies in dry films. Window inset: Relaxation time (τ) versus 1000/T; the same behavior has conductivity plot is displayed. *Source*: Reproduced with permission from González-Campos JB, García-Carvajal ZY, Prokhorov E, Luna-Bárcenas JG, Mendoza-Duarte ME, Lara-Romero J, Del Río RE, Sanchez IC. J Appl Polym Sci 2012;125:4082 [7]. Copyright 2012 John Wiley and Sons, Inc.

at which the characteristic relaxation time of the material equals about 100 s [91]. With this assumption and the calculated VFT parameters for dry PVA, we can determine a $T_g(\tau = 100\ \text{s}) = 43.7\,^{\circ}\text{C}$, which is in excellent agreement to those obtained with the $T_g = T_0 + 50$ K rule.

2.9.1 PVA Dielectric Relaxations Conclusions

Two VFT relaxations processes exist in PVA, depending on moisture conditions relaxations. Wet PVA shows two different VFT behaviors separated by the moisture evaporation region (from 80 to 120 °C), observed in the low (from 20 to

80 °C) and high temperature (above 120 °C) ranges. Previously, these two regions were erroneously assigned to two Arrhenius-type relaxations. While dry PVA shows a single α-relaxation non-Arrhenius, VFT-type relaxation clearly revealed after water evaporation.

REFERENCES

1. Morrel H, Grest GS. Phys Rev B 1979;20:1077.
2. Metatla N, Soldera A. Macromolecules 2007;40:9680.
3. Schut J, Bolikal D, Khan I, Pesnell A, Rege A, Rojas R, Sheihet L, Murthy NS, Kohn J. Polymer 2007;48:6115.
4. Dong Y, Ruan Y, Wang H, Zhao Y, Bi D. J Appl Polym Sci 2004;93:1553.
5. González-Campos JB, Prokhorov E, Luna-Bárcenas G, Mendoza-Galván A, Sanchez IC, Nuño-Donlucas SM, García-Gaitan B, Kovalenko Y. J Polym Sci B Polym Phys 2009;47:932.
6. González-Campos JB, Prokhorov E, Luna-Bárcenas G, Fonseca-García A, Sanchez IC. J Polym Sci B Polym Phys 2009;47:2259.
7. González-Campos JB, García-Carvajal ZY, Prokhorov E, Luna-Bárcenas JG, Mendoza-Duarte ME, Lara-Romero J, Del Río RE, Sanchez IC. J Appl Polym Sci 2012;125:4082.
8. Jadhav NR, Gaikwad VL, Nair KJ, Kadam HM. Asian J Pharm 2009;3:82.
9. Raju GG. *Dielectrics in Electrical Fields*. New York: Marcel Dekker Inc.; 2003.
10. Sorlier P, Viton C, Domard A. Biomacromolecules 2002;3: 1336.
11. Sato H, Ohtani H, Tsuge S, Aoi K, Takasu A, Okada M. Macromolecules 2000;33:357.
12. Kim SS, Kim SJ, Moon YD, Lee YM. Polymer 1994;35:3212.
13. Kim SS, Kim SH, Lee YM. J Polym Sci B Polym Phys 1996;34:2367.
14. Lee YM, Kim SH, Kim SJ. Polymer 1996;37:5897.
15. Ratto JA, Chen CC, Blumstein RB. J Appl Polym Sci 1996;59:1451.
16. Mucha M, Pawlak A. Thermochim Acta 2005;427:69.
17. Liu Y, Zhang R, Zhang J, Zhou W, Li S. Iran Polym J 2006;15:935.
18. Sakurai K, Maegawa T, Takahashi T. Polymer 2000;41:7051.
19. Pizzoli M, Ceccorulli G, Scandola M. Carbohydr Res 1991;222:205.
20. Einfeldt J, Meiβner D, Kwasniewski A. Prog Polym Sci 2001;26:1419.
21. Viciosa MT, Dionisio M, Silva RM, Mano JF. Biomacromolecules 2073;2004:5.
22. Huang RYM, Shieh JJ. J Appl Polymer Sci 1998:327. Huang RYM, Shieh JJ. Rad Phys Chem 2009;78:927.
23. Raju CHL, Rao JL, Reddy BCV, Brahmam KV. Bull Mater Sci 2007;30:215.
24. Lagashetty A, Havanoor V, Basavaraja S, Venkataraman A. Bull Mater Sci 2005;28:477.
25. Linares A, Nogales A, Rueda DR, Ezquerra TA. J Polym Sci B Polym Phys 2007;45:1653.
26. Lee YM, Kim SS. Korea Polymer J 1996;4:178.
27. Cendoya I, López D, Alegría A, Mijangos C. J Polym Sci B Polym Phys 1968;2001:39.
28. Bhargav PB, Sarada BA, Sharma AK, Rao VVRN. J Macromol Sci Pure Appl Chem 2010;46:131.
29. Migahed MD, Bakr NA, Abdel-Hamid MI, El-Hanafy O, El-Nimr M. J Appl Polym Sci 1995;59:655.
30. Hanafy TA. J Appl Polym Sci 2008;108:2540.
31. Singh KP, Gupta PN. Eur Polym J 1998;7:1023.
32. Ogura K, Tonosaki T, Shiigi H. J Electrochem Soc 2001;148:H21.
33. Hema M, Selvasekarapandian S, Arunkumar D, Sakunthala A, Nithya A. J Non-Cryst Solids 2009;355:84.
34. Harun MH, Saion E, Kassim A, Hussain MY, Mustafa IS, Omer MAA. Malaysian Polymer J 2008;3:27.
35. Agrawal SL, Awadhia A. Bull Mater Sci 2004;27:523.
36. Rajendran S, Sivakumar M, Subadevi R. Mater Lett 2004;58: 641.
37. Pissis P. Water in polymers and biopolymers by dielectric techniques. In: *Electromagnetic Aquametry*. Berlin Heidelberg: Springer; 2005.
38. Neto CGT, Giacometti JA, Job AE, Ferreira FC, Fonseca JLC, Pereira MR. Carbohydr Polym 2005;62:97.
39. Yu-Bey W, Shu-Huei Y, Fwu-Long M, Chung-Wei W, Shin-Shing S, Chih-Kang P, An-Chong C. Carbohydr Polym 2004;57:435.
40. M. Dionísio, N. M. Alves, J. F. Mano. e-polymers, 1618-7229. 2004, 044
41. Runt JP, Fitzgerald JJ. *Dielectric Spectroscopy of Polymeric Materials; fundamentals and applications*. Washington (DC): American Chemical Society; 1997.
42. Rowland SP. *Water in polymers*. Washington (DC): American Chemical Society; 1980.
43. Pezzin G. Polym Eng Sci 1978;18:821.
44. Köhler M, Lunkenheimer P, Loidl A. Eur Phys J 2008;E. 27:115.
45. Tsangaris GM, Psarras GC, Kouloumbi N. J Mater Sci 2027;1998:33.
46. Huang H, Yuan Q, Yang X. Colloids Surf B Biointerfaces 2004;39:31.
47. Wintle HJ. In: Bartnikas R, Eichorn RM, editors. *Engineering Dielectrics*. Volume IIA. Philadelphia (PA): ASTM Especial Technical Publication; 1983. p 239–354.
48. Khor E. *Chitin: Fulfilling a Biomaterials Promise*. Oxford, UK: Elsevier; 2001.
49. Mirzadeh H, Yaghobi N, Amanpour S, Ahmadi H, Mohagheghi MA, Hormozi F. Iran Polym J 2002;11:63.
50. Chandumpia A, Singhpibulporn N, Faroongsarng D, Sornprasit P. Carbohydr Polym 2004;58:467.

51. Zhang Y, Xue C, Xue Y, Gao R, Zhang X. Carbohydr Res 1914;2005:340.
52. Sung L, Du Y, Yang J, Shi X, Li J, Wang X, Kennedy JF. Carbohydr Polym 2006;66:168.
53. Andrade CT, Silva KMP, Tavares MI, Simão RA, Achete C, Pérez CA. J Appl Polym Sci 2002;83:151.
54. Balau L, Lisa G, Popa MI , Tura V, Melnig V. Cent Eur J Chem 2004;2:638–647.
55. Abthagir PS, Saraswathi R. Org. Electron 2004;5:299.
56. Ram MK, Gowri K, Malhotra BD. J Appl Polym Sci 1997;63: 141.
57. Bantikassegn W, Inganäs O. J Phys D Appl Phys 1996;29: 2971.
58. Lenzmann FO, O'Regan BC, Smits JJT, Kuipers HPCE, Sommeling PM, Slooff LH, van Roosmalen JAM. Prog Photovolt Res Appl 2005;13:333.
59. Bekkali AEH, Thurzo I, Kampen TU, Zahn DRT. Appl Surf Sci 2004;234:149.
60. Kremer F, Schönhals A, editors. *Broadband Dielectric Spectroscopy*. Berlin: Springer-Verlag; 2003.
61. Viciosa MT, Dionisio M, Mano JF. Biopolymers 2005;81:149.
62. Yagihara S, Yamada M, Asano M, Kanai Y, Shinyashiki N, Máximo S, Ngai KL. J Non-Cryst Solids 1998;235–237:412.
63. Kundu SK, Choe SG, Yamammoto W, Kita R, Yagihara S. Mater Res Soc Symp Proc 2007:1019.
64. Schwart GA, Bergman R, Wenson J. J Chem Phys 2004;120(12):5736.
65. Lu Y, Fujii M, Kanai H. Int J Food Sci Tech 1998;33:393.
66. Einfeldt J, Meiβner D, Kwasniewski A. J Non-Cryst Solids 2003;320:40.
67. Stickel F, Fischer EW, Richert R. J Chem Phys 2043;1996:104.
68. Cutroni M, Mandanici A. J Chem Phys 2001;114:7118.
69. Zhou J, Tzamalis G, Zaidi NA, Comfort NP, Monkman AP. J Appl Polym Sci 2001;79:2503.
70. Jousseaume V, Morsli M, Bonnet A. J Appl Polym Sci 1848;2002:84.
71. Ferrari L, Mott NF, Russo G. Philosophical Magazine 1989;59:263.
72. Schönhals A, Kremer F, Hofmann A, Fischer EW. Phys Rev Lett 1993;70:3459.
73. Garcia F, Garcia-Bernabe A, Compan V, Diaz-Calleja R, Guzman J, Riande E. J Polym Sci B: Polym Phys 2001;39:286.
74. Compan V, Guzman J, Diaz-Calleja R, Riande E. J Polym Sci B Polym Phys 1999;37:3027.
75. Lee AL, Wand AJ. Nature 2001;411:501.
76. Sokolov AP. Science, New Series 1996;273:1675.
77. Rasmussen BF, Stock AM, Ringe D, Petsko GA. Nature 1992;357:423.
78. Lazaridou A, Biliaderis CG. Carbohydr Polym 2002;48:179.
79. Toffey A, Glasser WG. Cellulose 2001;8:35.
80. Quijada-Garrido I, Iglesias-González V, Mazón-Arechederra JM, Barrales-Rienda JM. Carbohydr Polym 2007;68:173.
81. Kaymin IF, Ozolinya GA, Plisko YEA. Polym Sci 1980;22: 171.
82. Hodge RM, Bastow TJ, Edward GH, Simon GP, Hill AJ. Macromolecules 1996;29:8137.
83. Despond S, Espuche E, Cartier N, Domard A. J Polym Sci B Polym Phys 2005;43:48.
84. Ogura K, Kanamoto T, Itch M, Miyashiro H, Tanaka K. Polym Bull 1980;2:301.
85. Pizzoli M, Ceccorulli G, Scandola M. *Carbohydr Res*. 1991;222:205.
86. L.Y. Lim, E. Khor, C.E.J. Ling, *Biomed Mater Res* (*Appl Biomater*), 1999;48:111.
87. Machado AAS, Martins VCA, Plepis MG. *J Therm Anal Calorym*, 2002;67:491.
88. Balau L, Lisa G, Popa MI, Tura V, Melnig V. Cent Eur J Chem 2004;2:638.
89. Bhargav PB, Sarada BA, Sharma AK, Rao VVRN. J Macromol Sci Pure Appl Chem 2010;46:131.
90. Agrawal SL, Awadhia A. Bull Mater Sci 2004;27:523.
91. Saiter JM, Grenet J, Dargent E, Saiter A, Delbreilh L. Macromol Symp 2007;258:152.